Sir2 and Fun30 regulate ribosomal DNA replication timing via MCM helicase positioning and nucleosome occupancy

Carmina Lichauco[1^], Eric J. Foss[1^], Tonibelle Gatbonton-Schwager[1], Nelson F. Athow[1], Brandon Lofts[1], Robin Acob[1], Erin Taylor[1], James J. Marquez[1], Uyen Lao[1], Shawna Miles[1] and Antonio Bedalov[1,2*]

[1]Translational Science and Therapeutics Division, Human Biology Division, Fred Hutchinson Cancer Center, Seattle, WA

[2]Department of Biochemistry and Department of Medicine, University of Washington, Seattle, WA

[^]Carmina Lichauco and Eric J. Foss contributed equally to this work

[*]For correspondence: abedalov@fredhutch.org

Abstract

The association between late replication timing and low transcription rates in eukaryotic heterochromatin is well-known, yet the specific mechanisms underlying this link remain uncertain. In *Saccharomyces cerevisiae*, the histone deacetylase Sir2 is required for both transcriptional silencing and late replication at the repetitive ribosomal DNA arrays (rDNA). We have previously reported that in the absence of *SIR2*, a derepressed RNA PolII repositions MCM replicative helicases from their loading site at the ribosomal origin, where they abut well-positioned, high-occupancy nucleosomes, to an adjacent region with lower nucleosome occupancy. By developing a method that can distinguish activation of closely spaced MCM complexes, here we show that the displaced MCMs at rDNA origins have increased firing propensity compared to the nondisplaced MCMs. Furthermore, we found that both, activation of the repositioned MCMs and low occupancy of the adjacent nucleosomes critically depend on the chromatin remodeling activity of *FUN30*. Our study elucidates the mechanism by which Sir2 delays replication timing, and it demonstrates, for the first time, that activation of a specific replication origin *in vivo* relies on the nucleosome context shaped by a single chromatin remodeler.

Introduction

SIR2 is the founding member of a family of NAD-dependent protein deacylases called sirtuins, which have important effects on transcription, replication, chromatin structure and metabolism in organisms from yeast to humans (Houtkooper et al. 2012; Shahgaldi and Kahmini 2021). *SIR2* was initially identified in budding yeast in 1979 on the basis of its role in transcriptional repression at the silent mating type loci (Haber and George 1979; Klar et al. 1979; Rine et al. 1979), and it was therefore dubbed a "Silent Information Regulator". The silent mating type loci are heterochromatic regions that contain non-transcribed copies of the small open reading frames that determine yeast mating type, and deletion of *SIR2* not only activates their transcription but also abolishes their heterochromatic structure (Ivy et al. 1986; Rine and Herskowitz 1987; Weiss and Simpson 1998; Ravindra et al. 1999; Haber 2012). It was later discovered that, in addition to regulating transcription at the silent mating type loci, Sir2 also regulates DNA replication, and it does so not only at the silent mating type loci but also at the two other heterochromatic regions of the yeast genome, namely at telomeres and the rDNA (Pasero et al. 2002; Yoshida et al. 2014). It is this last activity of Sir2, namely its effect on replication at the rDNA, that is the focus of this report.

The rDNA, which encodes the structural RNA components of the ribosome, is composed of approximately 150 tandemly arranged 9.1 kb repeats (Woolford and Baserga 2013). At almost 1.4 megabases, the rDNA is too large to be replicated passively, and thus it must contain its own origins of replication. This is achieved by the organization shown in Figure 1A: The ribosomal RNAs are produced as two major species, known as the 35S and 5S, which are transcribed by RNA polI and RNA polIII, respectively (Fernandez-Pevida et al. 2015). Between the 5' ends of these genes is an origin of replication, and immediately to the left of this origin is a short Sir2-repressed RNA PolII-transcribed non-coding transcript called C-pro (Kobayashi and Ganley 2005; Li et al. 2006; Vasiljeva et al. 2008), which we will discuss further below. In wild-type cells, rDNA origins fire in the second half of S phase, making the rDNA among the later replicating regions of the genome, while in *sir2* mutants, they fire early in S phase (Pasero et al. 2002; Yoshida et al. 2014; Foss et al. 2017).

An indication of the biological significance of maintaining the late replication status of the rDNA came from a genome wide association study aimed at identifying naturally occurring genetic variants that affect replicative lifespan (Kwan et al. 2013). Replicative lifespan in budding yeast is defined as the number of daughter cells that a mother cell is able to produce and is therefore a measure of a cell's replicative capacity at birth. By measuring lifespan in segregants from a cross between two genetically diverse strains of yeast, Kwan et al. were able to identify a point mutation at the rARS that (1) decreased origin activity at the rDNA; (2) increased origin activity elsewhere in the genome; and (3) prolonged replicative lifespan. They interpreted these results as reflecting competition for replication resources between the origins in two distinct compartments of the nucleus, namely the heterochromatic repetitive nucleolus or rDNA and the non-repetitive sequences that make up the bulk of the yeast genome. This competition is exacerbated by the perturbation of nucleolar heterochromatin caused by the absence of *SIR2* (Yoshida et al. 2014; Foss et al. 2017). Most replication outside of the rDNA initiates from approximately 300 replication origins, and thus the 150 origins at the rDNA make up approximately one third of total origins. Increased replication resources directed toward the rDNA might therefore be expected to create a significant strain on replication in the rest of the genome.

Replication origins are known to compete for limiting resources at the level of origin firing. Broadly speaking, replication origin activity is regulated at two levels, namely origin licensing and origin firing (Remus and Diffley 2009). Origin licensing refers to loading of the replicative helicase in G1, and only origins that have been licensed are capable of being used in the subsequent S phase. Licensing occurs when an Origin Recognition Complex, Orc1-6, that is bound to an 11-17 base pair so-called ARS consensus sequence (ACS) within the origin loads two hexameric helicases, each consisting of a ring of subunits, MCM2-7, that encircles the DNA (Bell and Stillman 1992; Francis et al. 2009; Bell and Botchan 2013; Deegan and Diffley 2016; Deegan et al. 2016; Douglas et al. 2018; Lewis et al. 2022). The mechanism by which Orc recognizes origins and loads an MCM double-hexamer has been elucidated in great detail (Bell and Labib 2016; Costa and Diffley 2022; Hu and Stillman 2023). DNA replication initiates from only a subset of these licensed origins, namely those where the helicase complex is activated, a process referred to as origin firing (Rhind and Gilbert 2013). Origin firing is triggered by activation of two kinase signaling pathways, DDK and CDK, which then cause each hexameric MCM helicase to encircle

a single strand of DNA and track in opposite directions in front of the replisome, thereby establishing bidirectional replication (Heller et al. 2011; Larasati and Duncker 2016; Li et al. 2023). Firing factors are not present in sufficient quantities to activate all licensed origins simultaneously, and thus origins are activated in waves, with firing factors being recycled until the entire genome has been replicated (Mantiero et al. 2011; Tanaka et al. 2011). Determining the criteria by which origins are prioritized for activation remains an area of active research.

Importantly, if the competition between the origins at the rDNA and those in the rest of the genome is tilted in favor of the rDNA, either by a point mutation in the rARS or by deletion of *SIR2*, replication gaps between distantly spaced origins outside of the rDNA persist late into S phase, and genome duplication may remain incomplete when the cell enters mitosis (Foss et al. 2017). Indeed, the observation that weakening the rARS by a point mutation can suppress the short replicative lifespan characteristic of *sir2* mutants suggests that these replication gaps may be the ultimate cause of "replicative death". Teleologically, one can rationalize the prioritization of replication of the unique areas of the genome over the repetitive and heterochromatic areas, because (1) there are mechanisms available for repair in repetitive regions, like single-strand annealing, that are not available in unique regions, and they may therefore be able to survive lesions created when mitosis precedes the completion of replication; and (2) the cell is able to tolerate variation in copy number at the rDNA, but not deletion of protein-coding sequences in unique regions. Consistent with this view of the utility of assigning a low priority to replication of repetitive sequence, heterochromatic regions are also late-replicating in mammalian cells, and disease states have been associated with disruption of this pattern (Donley and Thayer 2013).

Despite its biological importance, the mechanism by which Sir2 suppresses replication initiation is poorly understood. Clues to Sir2's role in replication may be gleaned from its role in transcription, although here, too, our understanding is limited. Sir2's ability to repress transcription at the silent mating type loci has been postulated to follow from its role in chromatin compaction. Experiments demonstrating *SIR2*-dependent protection of heterochromatin from digestion with endonucleases or methylation by bacterial DNA methyltransferases support the notion that DNA in heterochromatin is generally less accessible (Gottschling 1992; Singh and Klar 1992; Loo and Rine 1994; Ansari and Gartenberg 1999). Thus, a widely publicized model attributes Sir2's ability

to inhibit transcription to blocking access of RNA PolII to the DNA, although a simple model of indiscriminate steric occlusion cannot account for this phenomenon (Chen and Widom 2005; Lynch and Rusche 2009; Kitada et al. 2012; Bondra and Rine 2023). Whether Sir2's effect on replication is similarly the result of chromatin compaction limiting access to enzymes involved in DNA metabolism is not known.

A study examining the distribution of MCM helicase complexes at the rDNA suggests that, rather than a global manifestation of lack of accessibility of the rDNA, the early activation of replication at the rDNA in the absence of Sir2 may reflect a more localized phenomenon (Foss et al. 2019). In this study, MCM binding was assessed at nucleotide-level resolution by fusing a subunit of MCM to micrococcal nuclease (MNase), a technique known as Chromatin Endogenous Cleavage, or "ChEC" (Figure 1B) (Schmid et al. 2004; Zentner et al. 2015). Permeabilization of cells with detergent followed by addition of calcium activates MNase, thereby generating approximately 65 base-pair fragments of DNA under MCM double-hexamers that can be identified by high-throughput sequencing. This analysis revealed that, while deletion of *SIR2* did not elicit an obvious change in the overall levels of licensing at the rDNA, it led to a dramatic redistribution of MCM helicase complexes: In wild-type cells, the helicase complexes are located almost exclusively immediately adjacent to a high occupancy well-positioned nucleosome approximately 130 base pairs to the left of the ACS. In contrast, the MCM complexes in *sir2* mutants are largely displaced to the right into an area with lower nucleosome occupancy (see Figure 1C and Figure 1-figure supplement 1). This displacement appears to be caused by the de-repression of C-pro transcription in the absence of *SIR2*, which results in RNA PolII pushing the MCM double-hexamer into the relatively nucleosome-free region. This observation is provocative in light of studies demonstrating that the arrangement of MCM-proximal nucleosomes can have a dramatic effect on MCM activation (Azmi et al. 2017). Specifically, by using chromatin remodeling enzymes (CREs) to create a variety of nucleosomal arrangements on an origin-containing fragment of DNA, Azmi et al. demonstrated that activation of an MCM double-hexamer loaded at that origin could be inhibited by nucleosomes arranged by specific CREs. In another study (Chacin et al. 2023), a mutant version of Orc1 that retains the ability to load MCM but alters phasing of MCM adjacent nucleosomes was shown to inhibit DNA replication *in vivo* and *in vitro*, consistent with a critical role for nucleosome organization at origins in the initiation of replication.

Taken together, the observations above led us to hypothesize that (1) relocation of MCM helicases from regions of high nucleosome occupancy to nearby regions of low nucleosome occupancy promotes early activation of replication origins in *sir2*; (2) this local difference in nucleosome occupancy is the result of modulation of nucleosomal architecture by one or more CREs; and therefore (3) screening CREs for the ability to suppress the early rDNA replication phenotype in *sir2* mutants might allow us to identify the relevant CRE. In this report, we show that the displaced MCM complexes fire before their nondisplaced counterpart and that increased nucleosome occupancy near the displaced MCMs in the absence of Fun30 CRE suppresses their early activation. This is the first *in vivo* demonstration of the modulation of an origin activity by a specific chromatin remodeler *in vivo*, and has implications for the broader relationship between transcription and replication timing.

Results

Fun30 chromatin remodeling activity is required for early rDNA replication in *sir2* mutant

To identify CREs required for the early replication of the rDNA in *sir2* mutants, we needed a method to determine replication timing, and for this we turned to S-seq. In this widely used technique, G1 and S phase populations of cells from a log phase culture are sorted using flow cytometry and their DNA subjected to genomic sequencing (Muller et al. 2014; Batrakou et al. 2020). Replication timing can then be inferred from read depths in the S phase fraction, because regions that replicate early in S phase will be present in two copies in most cells, while regions that replicate late will be present mostly as a single copy. S phase read depths are normalized to those in G1 to account for differences in DNA copy numbers, which is particularly important for repetitive loci whose copy number can vary, such as rDNA. As shown in Figure 2A, which depicts the S-seq profile of chromosome 12, relative replication timing (Trel) values using this approach typically range from 1.4 to 0.8 for early- and late-replicating regions, respectively, with a value of 1 indicating that a locus replicates at the same time as the genome-wide average (see Materials and Methods for specific calculation). The late replication of the rDNA, defined as coordinates 450,000 - 470,000 on chrXII, in wild type is reflected in a Trel value of 0.89, whereas this ratio increases to 1.2 upon deletion of *SIR2* (Figure 2A,B). Using this method, we showed that a point mutation in the ACS of the rARS suppresses early replication of the rDNA in *sir2*, while promoting

replication in the rest of the genome (Kwan et al. 2013; Foss et al. 2017). To identify potential chromatin remodelers required for early rDNA replication in *sir2*, we measured rDNA replication timing in double-mutants in *sir2* and each of 10 non-essential CRE subunits (Chd1, Fun30, Htl1, Irc5, Isw1, Isw2, Nhp10, Swp82). Deletion of *FUN30*, but no other gene, delayed replication of the rDNA in a *sir2* background, shifting the Trel value from 1.2 to 1.06, while having had no significant effect in *SIR2* cells (0.89 for WT and 0.91 for *fun30*) (Figure 2B).

Because Fun30 can form a complex with the replication scaffold protein Dpb11, it was possible that Fun30 played a structural rather than an enzymatic role in regulating rDNA replication. However, we found that a point mutation that abolishes Fun30 ATPase activity, K603R (Neves-Costa et al. 2009; Eapen et al. 2012), also suppresses early rDNA replication (Figure 2B), arguing that Fun30 instead promotes rDNA replication through its enzymatic activity in nucleosome remodeling. Fun30 is also known to play a role in the DNA damage response; specifically, phosphorylation of Fun30 on S20 and S28 by CDK1 targets Fun30 to sites of DNA breaks, where it promotes DNA resection (Chen et al. 2016; Bantele et al. 2017). To determine whether the replication phenotype that we observed might be a consequence of Fun30's role in the DNA damage response, we tested non-phosphorylatable mutants for the ability to suppress early replication of the rDNA in *sir2*; these mutations had no effect on the replication phenotype (Figure 2B), arguing against a primary role for Fun30 in DNA damage repair that somehow manifests itself in replication.

Fun30 **chromatin remodeling activity is required for maintaining rDNA array size in** ***sir2*** **mutant**

We next wanted to determine whether *FUN30* affects rDNA array size. The repetitive nature of the rDNA allows it to fluctuate in size, and mutations that impair DNA replication, either globally or in a manner specific to the rDNA, are associated with shrinkage of the rDNA. For example, the rDNA in a wild-type strain in the S288c background consists of 150 copies, but a point mutation at the ARS consensus sequence (ACS) that impairs Orc binding causes the rDNA to shrink to just 80 copies (Kwan et al. 2013). rDNA shrinkage in response to global replication defects is thought to reflect the fact that the rDNA, which typically comprises approximately 10% of genomic DNA,

imposes a significant replicative burden on the cell that can be ameliorated by decreasing the number of repeats (Salim et al. 2017).

We determined rDNA size by assessing the fraction of DNA sequencing reads from a sonicated G1 population that arose from the rDNA. While deletion of *FUN30* had no notable effect on rDNA size in a *SIR2* strain, it caused a 50% reduction in a *sir2* mutant, from 9.2% to 4.2% (Figure 2C). rDNA size reduction of a similar magnitude was observed in the ATPase-deficient Fun30K603R mutant, but not in the non-phosphorylatable Fun30S20AS28A mutant, mirroring the disparate effect of the two alleles on rDNA replication timing. The reduction of the rDNA size in *sir2 fun30* mutants was confirmed by qPCR analysis of DNA isolated from log cultures, and by Southern blots (Figure 2-figure supplement 1 and Figure 3). Based on measurements in log-growing cells, we estimated the rDNA size in *fun30 sir2* mutants to be ~40 repeats (Figure 2-figure supplement 1). This places it in a category comparable to the shortest rDNA arrays in a collection of DNA replication mutants noted for their contraction of the rDNA (Salim et al. 2017), thus emphasizing the severity of the replicative disadvantage conferred by the deletion of *FUN30* when Sir2 function is absent.

Alterations of rDNA size are promoted by the replication fork barrier (RFB), which imposes a unidirectional replication fork arrest to prevent head-to-head collisions between DNA polymerase and RNA polymerase I while transcribing 35S units. Replication forks that are stalled at the RFB are prone to breakage, which can lead to unequal sister chromatid exchange and fluctuations in rDNA array size. These rDNA size fluctuations are exacerbated in *sir2* mutants, which exhibit an increased rate of recombination, resulting in an unstable rDNA array size. Deletion of *FOB1*, which abolishes RFB function, stabilizes rDNA size by reducing,though not eliminating,the frequency of recombination-initiating double-strand breaks.

We have interpreted the shrinkage of the rDNA caused by deletion of *SIR2* and *FUN30* to be a specific example of the general phenomenon demonstrated by Salim et al. (Salim et al. 2017), i.e. that mutations that impair replication generate selective pressure that favors rDNA shrinkage. According to this interpretation, while deletion of *FOB1* is expected to retard the transition to reduced array sizes, it should not prevent it, and thus rDNA shrinkage should not be *FOB1*-dependent.

To determine whether the reduction of rDNA size in *sir2 fun30* mutants was dependent on RFB activity and *FOB1*, we deleted *FUN30* in a *sir2 fob1* strain with 160 repeats. Using this strategy, we obtained *fob1 sir2 fun30* transformants with over 150 rDNA repeats.. If rDNA shrinkage does not require Fob1, it should occur, albeit slowly, in *fob1* mutants. To assess this, we continuously grew several independent *fob1 sir2 fun30* colonies, along with control *fob1 sir2*, and *fob1 fun30* strains for 120 generations. We found that, unlike the control *fob1* strains, which maintained a stable rDNA size, all four *fob1 sir2 fun30* cultures reduced their rDNA arrays size to fewer than 100 copies by 120 division (Figure 2- figure supplement 2) . These results demonstrate that, although *FOB1* affects the kinetics of rDNA size reduction in *sir2 fun30* strains, the reduced rDNA array size upon *FUN30* deletion size does not depend on *FOB1*. Thus, suppressed rDNA replicaton drives the selection for reduced rDNA array size in both RFB-proficient and RFB-deficient *fun30 sir2* cells. Consistent with this notion, our S-seq results showed delayed rDNA replication timing in *fob1 sir2 fun30* cells with 150 rDNA repeats, compared to their *fob1 sir2* counterparts (Figure 2- figure supplement 3). In summary, we conclude that Fun30 nucleosome remodeling activity promotes rDNA replication and is required for maintaining rDNA size in *sir2* mutants. We next aimed to determine whether Fun30 exerts this effect by reducing MCM loading or the ability of loaded MCMs to fire.

High level of origin licensing at rDNA origins in WT, *sir2* and *sir2 fun30* mutants

It has been estimated that ~20% of potential rDNA origins are activated during any single S-phase in wild-type cells (Brewer and Fangman 1988; Linskens and Huberman 1988). Furthermore, single-molecule studies suggested that the fraction of active origins is increased in *sir2* mutant cells (Pasero et al. 2002; Yoshida et al. 2014). To determine whether *SIR2* and *FUN30* modulate rDNA replication by changing origin licensing, i.e. the fraction of origins that are bound by MCM helicase complexes prior to the beginning of S phase, we assessed licensing in WT, *sir2*, *fun30*, and *sir2 fun30* cells by measuring DNA cleavage by MCM2-MNase using Southern blots (Foss et al. 2021): Digestion with XmnI yields a 3.5 kb fragment that spans the rARS (Figure 3), and, if the rARS is licensed, activation of MNase by addition of calcium will eliminate this fragment, thus making it undetectable when using a probe upstream of the rARS. As a control, we used a fragment that, based on our MCM-ChEC data, should not contain MCM complexes. Activation of MNase

in all 4 genotypes led to an ~60-85% decrease in the XmnI fragment (Figure 3 and Figure 3 figure supplement 1), therefore we conclude that (1) licensing is high, at ~60-85%; and (2) a much higher fraction of origins are licensed than are activated, making it unlikely that significant regulation of origin activity occurs at the level of licensing. This is the first quantitative assessment of licensing at the rDNA in either wild type or *sir2*.

Fun30 promotes firing of rDNA origins and suppresses firing of non-rDNA origins in *sir2* mutants

Our observation that *FUN30* status had no obvious effect on rDNA origin licensing suggested that Fun30 might instead advance rDNA replication in sir2 mutants by promoting rDNA origin firing. To evaluate this possibility, we measured the effect of *FUN30* status on origin activity at the rDNA using 2D gels. We grew cells to log phase, arrested them for 1.5 hours in alpha factor and collected them at different time points after release into 200 mM hydroxyurea. Prior to separation on 2D gels, DNA was digested with NheI, which releases a 4.7 kb rARS-containing linear DNA fragment at the internal rDNA repeats (1N) and a much larger, 24.4 kb single-rARS-containing fragment originating from the rightmost repeat (Figure 4A). In 2D gels, active origins generate replication bubble arc signals, whereas passive replication of an origin appears as a y-arc (Figures 4B). Having a signal emanating from a single-rARS-containing fragment (Figures 4A and 4B) simplifies the comparison of rDNA origin activity in strains with different numbers of rDNA repeats, such as in *sir2* vs *sir2 fun30* mutants. Origin activity is expressed as a ratio of the bubble to the single-ARS signal, effectively measuring the number of active rDNA origins per cell at a given time point.

As seen previously, deletion of *SIR2* increased the number of activated rDNA origins, while deletion of *FUN30* suppressed this effect (Figure 4D). When analyzed in aggregate at 20, 30, 60 and 90 minutes following release into HU, the average number of activate rDNA origins in *sir2* mutant was increased 6.3-fold compared to those in WT (5.0±2.3 in *sir2* vs 0.8±0.4 in wt, $p<0.05$ by two-tailed t-test), and this increased number was reduced upon *FUN30* deletion (1.3±0.7 in *sir2 fun30*, $p<0.05$ by 2 tailed t-test vs *sir2,* NS for comparison to WT). Deletion of *FUN30* in a strain with a wild-type copy of *SIR2* did not have asignificant effect. We conclude that deletion

of *FUN30* partially reverses the accelerated activation of ribosomal origins caused by deletion of *SIR2*.

The overall impact of *FUN30* deletion on rDNA origin activity in a *sir2* background is expected to be a composite of two opposing effects: a suppression of rDNA origin activation and increased rDNA origin activation due to reduced rDNA size. To evaluate the effect of *FUN30* on rDNA origin activation independently of rDNA size, we generated an isogenic set of strains in a *fob1* background, all of which contain ~30 copies of the rDNA repeats. (Deletion of *FOB1* is necessary to stabilize rDNA copy number.) Comparing rDNA origin activity in *sir2* versus *sir2 fun30* genotypes, we observed a robust and reproducible reduction in rDNA origin activity upon *FUN30* deletion (Figure 4C). This finding confirms that the *FUN30* suppresses rDNA origin firing in *sir2* backgrpound independently of both rDNA size and *FOB1* status.

We and others have previously shown that deletion of *SIR2* not only advances replication at the rDNA but also retards replication elsewhere in the genome (Kwan et al. 2013; Yoshida et al. 2014). The absence of *SIR2* has been linked to decreased activation of less robust early replication origins, likely due to their heightened sensitivity to overall levels of replication-initiating factors. To ascertain the specificity of the interaction between *FUN30* and *SIR2*, we investigated whether deleting *FUN30* also mitigates the delayed activation of weak early origins in a *sir2* mutant background. We focused on the activation of ARS305, an origin we previously identified as delayed in a *sir2* mutant using 2D gel analysis. Overall, the comparison of origin activity at ARS305, measured as bubble arc to 1N signal, with that at rDNA demonstrates a reciprocial relationship between activity at ARS305 and rDNA across the four genotypes (Figure 4E). As seen previously, deletion of *SIR2* suppresses ARS305, whereas additional deletion of *FUN30* increased activity close to that of wild type. Deletion of *FUN30* in a *SIR2* background also showed a trend of increased origin activation, though this difference was not statistically significant.

Delayed initiation of genomic origins following *SIR2* deletion has been previously demonstrated on a global scale as a decline in the incorporation of a labeled uridine analogue, bromodeoxyuridine, at weak early origins in *sir2* cells compared to wild-type cells upon their release from G1 into HU (Yoshida et al. 2014). We employed a similar approach to investigate

whether the deletion of *FUN30* mitigates this effect, utilizing a different labeled nucleotide, ethynyl-deoxy-uridine (EdU), which can be isolated through click chemistry rather than immunoprecipitation. Wild-type (WT), *sir2*, *sir2 fun30*, and *fun30* cells engineered for the uptake and phosphorylation of the analogue (Viggiani and Aparicio 2006) were arrested in G1 using alpha factor and collected 60 minutes after release into medium containing HU and EdU. DNA extracted from these cells was sonicated and subjected to click chemistry with biotin azide to covalently link biotin to EdU incorporated into DNA. Biotinylated DNA was then purified and sequenced. The impact of *SIR2* and *FUN30* status on replication timing was assessed by graphing the EdU signal at 111 early origins in WT cells on the x-axis against the signal in *sir2*, *fun30*, and *sir2 fun30* cells on the y-axis (Figure 4F). Similar to observations with BrdU, we noted reduced EdU incorporation at a subset of early origins in *sir2* mutants, coupled with increased EdU incorporation at rDNA origins. Deletion of *FUN30* in a *sir2* background partially restored EdU incorporation at early origins, concomitant with reduced EdU incorporation at rDNA origins. In particular, the median value of $\log_{10}$ of read depths at 111 early origins, as the data are shown in Figure 4F, dropped from 6.5 for wild type to 6.2 for *sir2* but then returned almost to wild type levels (6.4) in *sir2 fun30*. The p value obtained by Student's t test, comparing the drop in 111 origins from wild type to *sir2* with that from wild type to *sir2 fun30* was highly significant ($<< 10^{-16}$) In contrast, *FUN30* deletion in the WT background did not reduce EdU incorporation at genomic origins (median 6.6). These findings highlight that *FUN30* deletion-induced suppression of rDNA origins in *sir2* is accompanied by the activation of genomic origins.

Early firing of displaced helicase complexes

While our results above demonstrate that deletion of *SIR2* promotes firing of rDNA origins and that additional deletion of *FUN30* suppresses this phenotype, they lack the resolution to distinguish replication arising from the displaced versus the nondisplaced MCM complexes. Other methods for measuring origin activation, such as generation of single-stranded DNA or incorporation of nucleoside analogs, also suffer from this limitation. Distinguishing between firing of the displaced versus the nondisplaced MCM complexes is important to test our hypothesis that displacement of the helicase complex into a relatively nucleosome-free region is responsible for its early activation. We therefore sought to devise a method that can differentiate activation of MCM complexes that

are only ~150 bp apart, i.e. the approximate distance between displaced and nondisplaced MCMs. We reasoned that, because MCM-ChEC has the resolution to distinguish closely spaced helicase complexes, the differential disappearance of such closely spaced footprints might permit us to distinguish their relative activation times.

To explore the possibility that the disappearance of the MCM-ChEC signal could be used to distinguish the firing of the displaced versus nondisplaced populations of MCM, we first asked whether the pattern of disappearance of the MCM signal recapitulates that of origin firing. In particular, while late origins are inhibited by hydroxyurea (HU), early origins are not; therefore, we asked whether this phenomenon was reflected in MCM-ChEC. To do this, we arrested cells in G1 using alpha factor and then released them into medium containing hydroxyurea (HU), taking samples for ChEC analysis at 15, 30, 45, 60 and 90 minutes (Figure 5A). HU inhibits ribonucleotide reductase and thereby dramatically slows S phase, making it easier to follow replication kinetics, but the relative order of firing of different origins remains unchanged. In Figure 5B, we plot the MCM-ChEC signal at 111 early origins and 101 late origins, with G1 on the x-axis and S phase on the y-axis. While we observed little difference in the signal abundance between early and late origins just 15 minutes after release from alpha factor, before origins have had a chance to fire, this difference increases over the time course, with early origins dropping more than late. MCM signal quantification demonstrates that the differences in MCM abundance between early and late origins increase over the time course in HU (Figure 5- figure supplement 1). Using chromatin immunoprecipitation followed by sequencing (ChIP-seq) for FLAG-tagged MCM2 in cells arrested in alpha factor and those released into HU for 60 minutes, we observed a similar reduction of the MCM signal at early compared to later origins, confirming our MCM-ChEC results (Figure 5-figure supplement 2). We conclude that the disappearance of the MCM-ChEC signal as cells progress through S phase can be used to assess origin firing.

We then turned our attention to the MCM signals at the rDNA origin; here the presence of the replication fork block approximately 1.5 kb from the sites of MCM binding provides a fortuitous means of confirming our interpretation, since the loss of the MCM-MNase signal at the origin should appear as a reciprocal increase where the replisome stalls. We first used MCM2-Flag ChIP in WT and sir2 cells after release into HU to confirm this prediction. In both WT and *sir2* cells, the MCM can be found at the rDNA origin in alpha factor-arrested cells as expected (Figure 5

figure supplement 3). However, at 60 minutes following release into HU, unlike in WT cells where the MCM signal remains at its loading site, in *sir2* mutants, we can see that a large fraction of the signal has now redistributed from its loading site and accumulated left of the RFB, consistent with early activation of rDNA origins in *sir2* cells and the arrest of the replicaiton forks at the RFB. While these results demonstrate that ChIP can be used to monitor the repositioning of the MCM signal at a kb scale and origin activation, its resolution is inadequate for small-scale changes in MCM signal distribution, which is needed to monitor the proposed differences in activation of repositioned and non-repositioned MCM complexes. We therefore turned to ChEC to address this question.

The MCM-ChEC signal in wild-type cells remained at their initial loading throughout the duration of the HU experiment (blue box in Figure 5C) as we have seen by ChIP in WT cells at 60 minutes. (Note that 200 mM HU causes an approximately 20-fold slowing of S phase, therfore a 60 minute time point is equivalent to <5 minutes without HU, i.e. prior to the time when the rDNA origin fires in wild-type cells). Like in wild type, this nondisplaced population of MCM in *sir2* remains relatively constant (blue box); however, in striking contrast, the displaced population of MCM in *sir2* (orange box) shows a continual decrease over the course of the experiment, and there is a concomitant increase in signal in the region upstream of RFB that is absent in wild type. Furthermore, both the decrease in the displaced signal (orange box) and its corresponding increase upstream of the RFB were suppressed by deletion of *FUN30*. The changes in the relative abundance of displaced and nondisplaced MCMs during the time course, as well as the repositioning of the MCM signal to the region upstream of RFB across different genotypes, were highly reproducible (Figure 5- figure supplement 4).

Taken together, these observations provide strong support for the hypothesis that the displaced population of MCM in *sir2* cells fires more readily than its nondisplaced counterpart and that the increased firing of the displaced MCMs is suppressed by *FUN30* deletion.

It is notable that, although a small fraction of the total G1 signal in wild type arises from the displaced location, this minor signal likewise disappears more rapidly than its nondisplaced counterpart (Figure 5- figure supplement 5). This suggests that some feature of the immediate chromatin environment may be responsible for the difference in firing times at the two locations,

and that this difference is present in both wild type and *sir2*; in other words, the fact that the displaced helicase complex is activated before the nondisplaced complex regardless of *SIR2* status is consistent with a model in which *sir2* mutants replicate their rDNA early by virtue of displacing much of their loaded helicases to a region where they are more apt to fire, rather than by altering the chromatin environment more globally to affect all replicative helicases in the nucleolus.

Finally, although deletion of *FUN30* could suppress replication initiation at the rDNA either by inhibiting the firing of the active, repositioned MCM complex or by preventing MCM repositioning to the "active location" in the first place, our results suggest that suppression occurs through the former mechanism. Consistent with previous reports that *fun30* mutants are deficient in transcriptional silencing (Neves-Costa et al. 2009), C-pro RNA levels were approximately twice as high in *sir2 fun30* cells compared to *sir2* cells when adjusted for rDNA size (Figure 5—figure supplement 6).

Moreover, deletion of *FUN30* shifts the distribution toward the repositioned MCM location over the non-repositioned one in G1 cells (Figure 5C), aligning with the increased C-pro transcription observed in *fun30* mutants. This shift is evident in both *sir2* and *SIR2* cells. Despite the increased transcription-mediated repositioning in *sir2 fun30* cells compared to *sir2* cells during G1, repositioned MCM persists longer in *sir2 fun30* cells than in *sir2* cells after release into HU. Additionally, *sir2 fun30* mutants exhibit reduced MCM accumulation at the RFB compared to *sir2* mutants after release into HU, supporting the conclusion that MCM disappearance in HU reflects origin activation rather than transcription-mediated displacement.

Fun30 maintains low nucleosome occupancy near repositioned MCMs

Our findings demonstrate that MCMs, when situated at their loading site adjacent to a high-occupancy +1 nucleosome, exhibit reduced firing propensity. In contrast, when these MCMs are displaced to a neighboring region with lower nucleosome occupancy, their firing propensity significantly increases. This heightened firing tendency is dependent on Fun30 CRE and its remodeling activity. This suggests that the absence of *FUN30* could elevate nucleosome occupancy around the relocated MCMs, consequently inhibiting their ability to fire.

To evaluate this possibility, we examined the effect of *FUN30* deletion on nucleosome occupancy at rDNA origins in WT and *sir2* background using MNase-seq in G1 arrested cells. Chromatin treatment with MNase digests DNA that is not bound by proteins, such as nucleosomes and transcription factors. Nucleosomes, which are wrapped by approximately 150 base pairs of DNA, tend to protect fragments in the 150-200 base pair range, and thus profiling fragments in this size range is widely used to assess nucleosome distribution. Plotting nucleosome midpoints at the rARS in G1 cells (Figure 6A and Figure 6-figure supplement 1) reveals that nucleosome occupancy at the +2 (green box) and +3 (red box) positions is higher in the *sir2 fun30* double mutant than in the *sir2* single mutant. Furthermore, this effect of Fun30 is not limited to the *sir2* background, since nucleosome occupancy is also modestly increased in *fun30* cells compared to wild type cells. These observations support the notion that it is the relatively nucleosome-free nature of the region into which MCMs are displaced in *sir2* that make the displaced complexes more prone to activation. Furthermore, this suggests that it could be particularly informative to assess nucleosome occupancy specifically adjacent to loaded MCM complexes, as described below.

It has previously been observed, both with MCM and with various transcription factors, that the ChEC technique can reveal not only the binding site of the protein to which the MNase is fused, but also, if present, that of the adjacent nucleosome (Zentner et al. 2015; Foss et al. 2019). This is due to the fact that the entrance and exit sites for DNA wrapped around a nucleosome are in close physical proximity, despite the fact that they are separated by approximately 150 base pairs, and thus the MNase fusion protein adjacent to a nucleosome often cleaves both sites. MCM-ChEC, therefore, provides a powerful tool for measuring nucleosome occupancy immediately adjacent to the MCM helicase complex *exclusively in those rDNA repeats where those complexes have been loaded*. By plotting the midpoints of 150-200 bp fragments released by MCM2-Mnase, we were able to determine that nucleosome occupancy at both the +2 and +3 nucleosomes, i.e. those adjacent to the displaced MCM complexes, are elevated in *sir2 fun30* as compared to *sir2* (Figure 6B and Figure 6- figure supplement 1). This finding indicates that Fun30 is required for maintaining the low nucleosome occupancy in the region into which the preponderance of MCM complexes have been displaced in *sir2* mutant cells.

Discussion

In this study, we have attempted to shed light on the mechanism by which Sir2 represses replication origins at the rDNA. Sir2's activity has been widely ascribed to the intuitive, but mechanistically imprecise, notion that "closed chromatin" is less accessible to both transcription and replication factors. Consistent with this model, deletion of *SIR2* abolishes heterochromatic compaction and simultaneously increases the ability of methylases and restriction endonucleases to act on those sequences (Gottschling 1992; Singh and Klar 1992; Loo and Rine 1994; Weiss and Simpson 1998; Ansari and Gartenberg 1999; Ravindra et al. 1999). However, at least in its simplest form, non-specific steric exclusion of DNA metabolic enzymes cannot fully account for the suppression of transcription and replication at the rDNA. Steric arguments such as these are even less compelling when made for rDNA than for the silent mating type loci and telomeres, because chromatin compaction has been studied mostly in the context of the complete Sir complex (Sir2-4) (Gartenberg and Smith 2016). In contrast, Sir3, and Sir4 are not present at the rDNA (Straight et al. 1999). Moreover, rDNA is the most highly transcribed region of the genome, with transcription by PolI and PolIII accounting for approximately 80% of cellular RNA (Warner 1999; Woolford and Baserga 2013). These two polymerase complexes are similar in size to the PolII complex, thus size alone is not sufficient to selectively occlude PolII.

Additionally, deletion of SIR2 increases accessibility of restriction enzymes to heterochromatin at the HML locus by 1.5-fold, yet it increases PolII transcription by over 3000-fold (Holland 2002). This indicates that the magnitude of Sir2's steric exclusion is insufficient to explain its effect on PolII transcription. Similar measurements in eukaryotic cells found little difference in accessibility of restriction enzymes and micrococcal nuclease between euchromatin and heterochromatin (Chereji et al. 2019).

In the current report, we argue that Sir2's role in suppressing replication at the rDNA reflects local differences in the distribution of the MCM replicative helicase complexes rather than more global occlusion of these complexes from the rDNA. In particular, our results suggest that the key difference between wild type and *sir2*, with regard to replication initiation, is the location of the MCM complex, with the preponderance of that complex in wild type abutting a high-occupancy nucleosome while, in *sir2*, it is mostly in a relatively nucleosome-free region. Furthermore, we

show that, even though this nucleosome-free region is less than 200 base pairs from MCM's original location, the displaced helicase complex is significantly more prone to activation than its nondisplaced counterpart. Moreover, the chromatin-remodeling enzyme Fun30 is required to maintain the nucleosome-free character around the displaced MCM, and its deletion both increases nucleosome occupancy and decreases the ability of the displaced MCM to fire. Finally, as discussed below, we suggest that the increased proclivity of the displaced MCM to fire is not an anomaly specific to the physiology of *sir2* cells, but is an integral feature of replication of the rDNA during normal S phase.

Our model for the manner in which Sir2 regulates rDNA replication depends critically on the notion that the local nucleosome landscape can influence the activation of MCM helicase complexes (Figure 7), and *in vitro* experiments suggest that this is, indeed, the case (Azmi et al. 2017): Azmi et al. monitored both licensing and firing *in vitro*, using a 3.8 kb nucleosomal template containing the ARS1 origin. They found that, while licensing was equivalent whether the template had been populated with nucleosomes using Swi/Snf or Rsc remodelers, on the one hand, or Isw1a, on the other, the loaded MCM complexes in the latter templates were more prone to activation. Furthermore, MCM complexes on Swi/Snf- or Rsc-remodeled templates could be made more prone to activation if subsequently treated with Isw1a, although the converse was not true. The salient difference between the two types of nucleosomal landscapes, however, was not obvious, as the distance between the MCM complex and the nearest nucleosome was not notably affected, although it is possible that the composition (e.g. H2A/H2B content) differs. It was also unclear how the nucleosome landscape affected activation of MCM complexes, though the relevant step in activation was determined to be the formation of the CMG complex with Cdc45 and GINS rather than the prior phosphorylation of the complex by DDK. In summary, while it is clear that the local nucleosome landscape can affect origin activity (Eaton et al. 2010; Belsky et al. 2015), the underlying mechanism remains murky.

Regardless of the reason for the increased proclivity of the displaced MCM to fire, the observation has implications for replication at the rDNA not only in *sir2* mutants but also in wild type. We have previously shown that the rightward displacement of MCM double hexamers in *sir2* is due to derepression of C-pro transcription (Foss et al. 2019), while our current results demonstrate that

the displaced MCM is more prone to activation. Combining these two observations, we suggest that the rDNA replicates earlier in *sir2* than in wild type simply because more of the MCM complex is in a location that favors its activation; in other words, we favor the view that the region of relatively low nucleosome occupancy to the right of MCM's normal location is more amenable to MCM activation, regardless of *SIR2* status. In support of this notion, close analysis of our MCM-ChEC data reveals that, while MCM complexes at the displaced location are much rarer in wild type than they are in *sir2*, this particular subpopulation appears equally susceptible to activation in both genotypes. This has the important implication that the manner in which the rDNA origin fires in *sir2* mutants may be simply an exaggerated instance of its normal behavior, and that even in wild type cells, it is predominantly from MCMs that are displaced, likely due to low level of C-pro transcription, that replication initiates.

Classic studies that employed EM and two-dimensional gel electrophoresis showed that only a fraction of rDNA origins, estimated at one in five, are activated in any single cell cycle in yeast (Brewer and Fangman 1988; Linskens and Huberman 1988). These estimates were later corroborated by single molecule analysis, which also observed that the fraction of active origins increases in *sir2* mutants (Pasero et al. 2002). This low fraction of active rDNA origins could be due to insufficient origins licensing, suppression of activation or licensed origins or a combination of the two mechanisms. Our measurements of rDNA licensing showed that MCM are loaded in up to 90% of origins in WT cells and allowed us to conclude that regulation or rDNA replication initiation occurs primarily at the level of origin firing.

Chromatin remodeling enzymes have been proposed to assist DNA replication by modulation of nucleosome phasing in the vicinity of replication origins, but it has proven difficult to assign specific roles to remodelers in genome replication *in vivo* (Cutler et al. 2018). One of the reasons for this difficulty is the redundancy among different remodelers on one hand, and the multiple essential roles CRE play in DNA transactions in addition to replication. For example, *in vitro* studies have identified four different remodelers that in combination with ORC can phase nucleosome at 320 replication origins (Chacin et al. 2023). However, a deletion of any single of these remodelers had no discernable effect on nucleosome phasing *in vivo* and a quadruple mutant was required to abolish phasing. While the characterization of this quadruple mutant suggested

impaired replication initiation, it was difficult to exclude indirect effects that might have been caused by the effects on transcription. In contrast, the effect of a chromatin remodeler on DNA replication we describe in this work is remarkably specific: we found that the activity of a single remodeler, Fun30, is required to activation not only of a specific origin, but that its action is specific to nucleosomes adjacent to repositioned MCM complexes at the rDNA. The suppression of rDNA origin activity in sir2 mutants, which contained a large fraction of repositioned MCMs, by *FUN30* deletion is so severe that it reduces the rDNA size ~3-5 fold, from 160 to 35-50 copies.

In conclusion, our findings contribute to a growing body of evidence highlighting the importance of positioning of the MCM replicative helicase within the local nucleosome environment in determining replication timing (Azmi et al. 2017; Rodriguez et al. 2017). While it is clear that small differences in this positioning can have significant effects on the timing of DNA replication, it is unlikely that a simple rule exists to directly infer origin timing solely based on the distance between the MCM complex and the nearest nucleosome. Nonetheless, our results suggest that this parameter could be a crucial piece of the puzzle in understanding why some origins fire early in S phase, while others fire late. Further research is needed to unravel the precise molecular mechanisms governing the interplay between the MCM complex and nucleosomes and how these dynamics influence replication timing across different genomic loci. Such insights will deepen our understanding of DNA replication regulation in the context of disease states associated with epigenetic drift, such as aging and cancer.

Material and methods

Yeast strain

Strains used in the study were derived from BY4741 and W303 and are provided in Suplemental Table 1. Cells were grown in standard yeast peptone 2% dextrose media except for hydroxyurea time course study which employed synthetic media.

Strains containing point mutations in FUN30 were made using a plasmid that contains CAS9 and gRNA targeting the PAM sites adjacent to the desired mutation sites in *FUN30* as described. Oligos containing FUN30-targeting gRNAs were cloned into pML104. pML104 was a gift from John Wyrick (Addgene plasmid # 67638)(Laughery et al. 2015). The plasmids, which induce double strand breaks within FUN30, were co-transformed with DNA blocks containing the repair

templates with the desired mutations and altered PAM sites, synthetically synthesized by IDT. *FUN30* DNA was PCR amplified from the resulting transformants and sequenced to verify that the desired mutations have been introduced.

Edu-incorporating yeast strains were derived from W303 and contain four Brdu vectors that express HSV-TK and hENT1 ((Viggiani and Aparicio 2006). Plasmids containing BrdU cassete obtained from Addgene (Addgene plasmid # 71789-71792), were integrated at four different auxotrophic loci (*HIS3, TRP1, LEU2*, and *URA3*). Single integration of each Brdu cassette was confirmed via PCR using plasmid-specific primer sets as described ((Viggiani and Aparicio 2006), which assured that the strains contain exactly four copies of the BrdU cassette

Measurements of rDNA replication timing using S-seq

S-seq experiments were carried out as previously described (Foss et al. 2017). Cells were grown to log phase in YEPD media, fixed using 70% (vol/vol) ethanol, subjected to proteinase K digestion, and their DNA stained with Sytox Green as described (Foss 2001). Cells were sorted according to DNA content on a BD Biosciences FACSAria II cell sorter into G1 and S fractions. DNA from a minimum of 1 e-6 cells from each fraction was isolated using the YeaStar Genomic DNA Kit (Zymo Research). DNA was fragmented by sonication and sequenced.

MNase seq

We carried out MNase-Seq as previously described (Foss 2019). Briefly, cells grown to log phase in rich medium, Yeast Peptone Agar with 2% glucose (YEPD), from an overnight 25 mL culture were synchronized with 3 µM alpha-factor for 1.5 hrs. at 30˚C. Arrested cells were crosslinked with 1% formaldehyde for 30 min at room temperature water bath with shaking. Formaldehyde was quenched with 125 mM glycine and cells were centrifuged at 3000 rpm for 5 min. Cells were washed twice with water and resuspended in 1.5 mL Buffer Z (1 M sorbitol, 50 mM Tris-HCl pH 7.4) with 1 mM beta-mercaptoethanol (1.1 µL of 14.3 M beta-mercaptoethanol diluted 1:10 in Buffer Z) per 25 mL culture. Cells were treated with 100 µL 20 mg/ mL zymolyase at 30˚C for 20–30 min. Spheroplasts were centrifuged at 5000 rpm for 10 min and resuspended in 5 mL NP buffer (1 M sorbitol, 50 mM NaCl, 10 mM Tris pH 7.4, 5 mM $MgCl_2$, 1 mM $CaCl_2$) supplemented with 500 µM spermidine, 1 mM beta-mercaptoethanol and 0.075% NP-40. Nuclei were aliquoted in tubes with varying concentrations of micrococcal nuclease (Worthington), mixed via tube

inversion, and incubated at room temperature for 20 mins. Chromatin digested with 1.9 U– 7.5 U micrococcal nuclease per 1/5th of spheroplasts from a 25 mL culture yielded appropriate mono-, di-, tri- nucleosome protected fragments for next-generation sequencing. Digestion was stopped with freshly made 5x stop buffer (5% SDS, 50 mM EDTA) and proteinase K was added (0.2 mg/ml final concentration) for an overnight incubation at 65˚C to reverse crosslinking. DNA was extracted with phenol/chloroform and precipitated with ethanol. Micrococcal nuclease digestion was analyzed via gel electrophoresis prior to proceeding to library preparation. Sequencing libraries were prepared as described below for ChEC.

Chromatin Endogenous Cleavage (ChEC)

ChEC-seq was carried out as previously described (Foss et al. 2019; Foss et al. 2021). Briefly, MNase was activated by addition of CaCl2 to cells that were permeabilized with digitonin. DNA was extracted from cells using phenol and chloroform, precipitated using salt and ethanol and used to construct sequencing libraries without size fractionation. Cells were centrifuged at 1,500 x g for 2 mins, and washed twice in cold Buffer A (15 mM Tris pH 7.5, 80 mM KCl, 0.1 mM EGTA) without additives. Washed cells were carefully resuspended in 570 µL Buffer A with additives (0.2 mM spermidine, 0.5 mM spermine, 1 mM PMSF, ½ cOmplete ULTRA protease inhibitors tablet, Roche, per 5 mL Buffer A) and permeabilized with 0.1% digitonin in 30˚C water bath for 5 min. Permeabilized cells were cooled at room temperature for 1 min and 1/5th of cells were transferred in a tube with freshly made 2x stop buffer (400 mM NaCl, 20 mM EDTA, 4 mM EGTA)/1% SDS solution for undigested control. Micrococcal nuclease was activated with 5.5 µL of 200 mM $CaCl_2$ at various times (5 mins, and 10 mins) and the reaction stopped with 2x stop buffer/1% SDS. Once all time points were collected, proteinase K was added to each of the collected time points and incubated at 55˚C water bath for 30 mins. DNA was extracted using phenol/chloroform and precipitated with ethanol. Micrococcal nuclease digestion was analyzed via gel electrophoresis prior to proceeding to library preparation. Library was prepared as previously described used using total DNA, without any fragment size selection (Foss et al. 2019; Foss et al. 2021).

Chromatin immunoprecipitation followed by sequencing (ChIP-seq)

Cells were grown to log phase in rich medium, YEPD (1% Yeast Extract, 2% Peptone, 2% glucose), synchronized with 3 μM alpha-factor for 1.5 hrs. at 30°C. G1 arrested cells were released into 200 mM hydroxyurea (HU) YEPD and grown for 1hr. Cells were crosslinked with 1% formaldehyde for 30 min at room temperature, quenched with 125 mM glycine for 5 minutes, and centrifuged at 3000 rpm for 5 minutes. Cell pellets were washed three times with TBS (20 mM Tris-HCl, pH 7.6, 150 mM NaCl). Cell pellets were flash frozen.

Chromatin Preparation: The cell pellet was thawed in 300 μL Breaking Buffer (100 mM Tris-HCl, pH 8.0, 20% Glycerol) supplemented with protease inhibitors (Pierce Protease inhibitor EDTA-free tablets [Thermo Scientific A32965] and 1 mM PMSF). 300 μL acid-washed glass beads were added to the mixture. Cells were lysed using a BioSpec Mini-Bead-beater in a cold room: 5x 30-second pulses with 1-minute on ice between rounds. The supernatant was transferred to a new tube and added 600 μL FA buffer (50 mM Hepes-KOH, pH 7.6, 150 mM NaCl, 5 mM EDTA, 1% Triton X-100, 0.1% Sodium deoxycholate) with protease inhibitors. The chromatin was sonicated with a F60 Sonic Dismembrator 10 times for 10 seconds at setting 4, with 1-minute rests on ice between rounds. The sonicated chromatin was centrifuged at 14,000 rpm for 15 minutes at 4°C. The supernatant was transferred and spun again at 14,000 rpm for 15 minutes at 4°C.

Immunoprecipitation (IP): For IP, 20 μL of Dynabeads Protein G beads (Invitrogen 10004D) were washed three times with 500 μL PBS-T (0.8% NaCl, 0.144% Na_2HPO_4, 0.02% KCl, 0.024% KH_2PO, 0.1% Tween 20, pH 7.1), resuspended in PBS-T, and incubated with 5 μL of FLAG M2 (Sigma F1804) antibody for 60 minutes at room temperature. The antibody-conjugated beads were washed and resuspended in 20 μL FA buffer with protease inhibitors. IP chromatin samples (1 μg) were brought up to 400 μL with FA buffer with protease inhibitors and incubated with antibody-conjugated beads for 90 minutes at room temperature. Beads were washed three times with FA buffer with protease inhibitors, twice with FA-HS buffer (50 mM Hepes-KOH, pH 7.6, 500 mM NaCl, 5 mM EDTA, 1% Triton X-100, 0.1% Sodium deoxycholate with protease inhibitors), and once with RIPA buffer (10 mM Tris-HCl, pH 8.0, 0.25 M LiCl, 0.5% NP-40, 0.5% Sodium deoxycholate, 5 mM EDTA with protease inhibitors). Input sample was generated by adding 0.1

μg chromatin in 40 μL FA buffer to 40 μL 2X Stop buffer (20 mM Tris-HCl, pH 8.0, 100 mM NaCl, 20 mM EDTA, 1% SDS, 2% Tween 20) and reversed crosslinks by overnight incubation at 65°C.

Elution and Crosslink Reversal: Bound chromatin was eluted by incubating the beads in 80 μL 2X Stop buffer at 75°C for 10 minutes. The eluate was collected, and crosslinks were reversed by overnight incubation at 65°C. The IP and Input were treated with 4 μL of 20 mg/mL RNase A and incubated at 55°C for 1 hour, followed by 4 μL of 20 mg/mL Proteinase K and incubation at 55°C for at least 3 hours. DNA was purified using a MinElute PCR Purification Kit

Paired-Ends NGS: Chromatin immunoprecipitation samples were prepared for sequencing following the protocol for the Kapa Hyper Kit. For Input samples, 2 ng were processed for End Repair. For IP samples, the entire volume was used. PCR amplification was performed with 10-14 cycles based on DNA quantity.

Quantification of rDNA replication using the thymidine analogue EdU

Cells were grown to log phase in rich YEPD medium from a 50 mL culture and synchronized in G1 using 3 μM alpha factor for 2 hours at 30°C. Using 500 μg/mL pronase, arrested cells were released into rich media containing 200 mM hydroxyurea and 130 μM EdU (5-Ethynyl-2'-deoxyuridine). Cells were harvested in G1 and after 60 minutes released into HU. DNA was extracted using YeaStar Genomic DNA Kit (Zymo Research) and sonicated. Separate sequencing primers were ligated to each of the samples. Samples were pooled together, and subjected to click chemistry reaction in 10 mM Tris pH 7.4, 50mM NaCl, 20 μM biotin-TEG azide (Vector Laboratories), 5mM THPTA (tris-hydroxypropyltriazolylmethylamine) (Vector Laboratories), 1mM copper sulfate, and 15 mM sodium ascorbate (total volume 200 μL). Click reaction proceeded for 30 minutes at room temperature prior to DNA ethanol precipitation. Streptavidin magnetic beads (New England Biolabs) were washed 3 times with B&W buffer I (100 mM NaCl, 10 mM Tris-HCl pH 8.0, 1 mM EDTA, 0.05% Tween20, 0.5% SDS) before adding 100 μL of bead suspension to 180 μL DNA plus B&W buffer I. After a 30-minute incubation at room temperature while gently inverting tubes, bead bound DNA was washed with 200 μL B&W buffer I followed by 100 μL Stringency wash buffer (0.1% SDS, 0.1% SSC buffer) and 200 μL Wash Buffer II (100

mM NaCl, 10 mM Tris-HCl pH 8.0, 1 mM EDTA, 0.05% Tween 20). DNA was eluted off the beads by denaturation at 98°C for 5 minutes, followed by cooling at 25°C. Edu-labeled DNA was PCR amplified post-pulldown and subjected to sequencing.

Hydoxyurea ChEC time course experiment

Cells grown in synthetic media to logarithmic phase were arrested in G1 using alpha factor for 90 minutes, centrifuged, washed in water to remove alpha factor, and released into media containing 200 mM Hydroxyurea. Cells were harvested in G1 and at indicated time points following release into HU-containing media, chilled at 4 degrees and analyzed by ChEC as described above.

qRT-PCR analysis of c-pro transcript and rDNA copy number

RNA was extracted from logarithmically growing cells after spheroplasting using an RNA-Easy column. The sequences of the primers used in qRT-PCR for c-pro and PDA1 mRNA are provided in Supplemental Table 2. rDNA size was measured by qPCR using DNA that was extracted by phenol-chloroform extraction and ethanol precipitation using the primers listed in As an internal standard, qPCR was done in parallel on the DNA extracted from *fob1* strains with 180 and 35 rDNA copies whose rDNA sizes had been verified by Pulsed Field Gel Electrophoresis (Kwan et al. 2023).

ChEC Southern blots for measuring origin licensing

Cells carrying MCM2-Mnase were subjected to ChEC as described above, except that the stop SDS was omitted from the stop buffer to allow subsequent spheroplasting. DNA was extracted from spheroplasts using the YeaStar Genomic DNA Kit (Zymo Research), digested with XmnI, separated on 1.75% agarose gels and analyzed by standard Southern blotting technique. The primers used to make the rDNA and *PIK1* control probe are listed in Supplemental Table 2.

Ackowledgements

We thank Toshi Tsukiyama, Bonny Brewer and M.K. Raghuraman for yeast strains. Research reported in this publication was supported by the National Institute of General Medical Sciences of the National Institutes of Health under Award Number R01GM117446.

References

Ansari A, Gartenberg MR. 1999. Persistence of an alternate chromatin structure at silenced loci in vitro. *Proc Natl Acad Sci U S A* **96**: 343-348.

Azmi IF, Watanabe S, Maloney MF, Kang S, Belsky JA, MacAlpine DM, Peterson CL, Bell SP. 2017. Nucleosomes influence multiple steps during replication initiation. *Elife* **6**.

Bantele SC, Ferreira P, Gritenaite D, Boos D, Pfander B. 2017. Targeting of the Fun30 nucleosome remodeller by the Dpb11 scaffold facilitates cell cycle-regulated DNA end resection. *Elife* **6**.

Batrakou DG, Muller CA, Wilson RHC, Nieduszynski CA. 2020. DNA copy-number measurement of genome replication dynamics by high-throughput sequencing: the sort-seq, sync-seq and MFA-seq family. *Nat Protoc* **15**: 1255-1284.

Bell SD, Botchan MR. 2013. The minichromosome maintenance replicative helicase. *Cold Spring Harb Perspect Biol* **5**: a012807.

Bell SP, Labib K. 2016. Chromosome Duplication in Saccharomyces cerevisiae. *Genetics* **203**: 1027-1067.

Bell SP, Stillman B. 1992. ATP-dependent recognition of eukaryotic origins of DNA replication by a multiprotein complex. *Nature* **357**: 128-134.

Belsky JA, MacAlpine HK, Lubelsky Y, Hartemink AJ, MacAlpine DM. 2015. Genome-wide chromatin footprinting reveals changes in replication origin architecture induced by pre-RC assembly. *Genes Dev* **29**: 212-224.

Bondra ER, Rine J. 2023. Context-dependent function of the transcriptional regulator Rap1 in gene silencing and activation in Saccharomyces cerevisiae. *Proc Natl Acad Sci U S A* **120**: e2304343120.

Brewer BJ, Fangman WL. 1988. A replication fork barrier at the 3' end of yeast ribosomal RNA genes. *Cell* **55**: 637-643.

Chacin E, Reusswig KU, Furtmeier J, Bansal P, Karl LA, Pfander B, Straub T, Korber P, Kurat CF. 2023. Establishment and function of chromatin organization at replication origins. *Nature* **616**: 836-842.

Chen L, Widom J. 2005. Mechanism of transcriptional silencing in yeast. *Cell* **120**: 37-48.

Chen X, Niu H, Yu Y, Wang J, Zhu S, Zhou J, Papusha A, Cui D, Pan X, Kwon Y et al. 2016. Enrichment of Cdk1-cyclins at DNA double-strand breaks stimulates Fun30 phosphorylation and DNA end resection. *Nucleic Acids Res* **44**: 2742-2753.

Costa A, Diffley JFX. 2022. The Initiation of Eukaryotic DNA Replication. *Annu Rev Biochem* **91**: 107-131.

Cutler S, Lee LJ, Tsukiyama T. 2018. Chromatin Remodeling Factors Isw2 and Ino80 Regulate Chromatin, Replication, and Copy Number of the Saccharomyces cerevisiae Ribosomal DNA Locus. *Genetics* **210**: 1543-1556.

Deegan TD, Diffley JF. 2016. MCM: one ring to rule them all. *Curr Opin Struct Biol* **37**: 145-151.

Deegan TD, Yeeles JT, Diffley JF. 2016. Phosphopeptide binding by Sld3 links Dbf4-dependent kinase to MCM replicative helicase activation. *EMBO J* **35**: 961-973.

Donley N, Thayer MJ. 2013. DNA replication timing, genome stability and cancer: late and/or delayed DNA replication timing is associated with increased genomic instability. *Semin Cancer Biol* **23**: 80-89.

Douglas ME, Ali FA, Costa A, Diffley JFX. 2018. The mechanism of eukaryotic CMG helicase activation. *Nature* **555**: 265-268.

Eapen VV, Sugawara N, Tsabar M, Wu WH, Haber JE. 2012. The Saccharomyces cerevisiae chromatin remodeler Fun30 regulates DNA end resection and checkpoint deactivation. *Mol Cell Biol* **32**: 4727-4740.

Eaton ML, Galani K, Kang S, Bell SP, MacAlpine DM. 2010. Conserved nucleosome positioning defines replication origins. *Genes Dev* **24**: 748-753.

Fernandez-Pevida A, Kressler D, de la Cruz J. 2015. Processing of preribosomal RNA in Saccharomyces cerevisiae. *Wiley Interdiscip Rev RNA* **6**: 191-209.

Foss EJ. 2001. Tof1p regulates DNA damage responses during S phase in Saccharomyces cerevisiae. *Genetics* **157**: 567-577.

Foss EJ, Gatbonton-Schwager T, Thiesen AH, Taylor E, Soriano R, Lao U, MacAlpine DM, Bedalov A. 2019. Sir2 suppresses transcription-mediated displacement of Mcm2-7 replicative helicases at the ribosomal DNA repeats. *PLoS Genet* **15**: e1008138.

Foss EJ, Lao U, Dalrymple E, Adrianse RL, Loe T, Bedalov A. 2017. SIR2 suppresses replication gaps and genome instability by balancing replication between repetitive and unique sequences. *Proc Natl Acad Sci U S A* **114**: 552-557.

Foss EJ, Sripathy S, Gatbonton-Schwager T, Kwak H, Thiesen AH, Lao U, Bedalov A. 2021. Chromosomal Mcm2-7 distribution and the genome replication program in species from yeast to humans. *PLoS Genet* **17**: e1009714.

Francis LI, Randell JC, Takara TJ, Uchima L, Bell SP. 2009. Incorporation into the prereplicative complex activates the Mcm2-7 helicase for Cdc7-Dbf4 phosphorylation. *Genes Dev* **23**: 643-654.

Gartenberg MR, Smith JS. 2016. The Nuts and Bolts of Transcriptionally Silent Chromatin in Saccharomyces cerevisiae. *Genetics* **203**: 1563-1599.

Gottschling DE. 1992. Telomere-proximal DNA in Saccharomyces cerevisiae is refractory to methyltransferase activity in vivo. *Proc Natl Acad Sci U S A* **89**: 4062-4065.

Haber JE. 2012. Mating-type genes and MAT switching in Saccharomyces cerevisiae. *Genetics* **191**: 33-64.

Haber JE, George JP. 1979. A mutation that permits the expression of normally silent copies of mating-type information in Saccharomyces cerevisiae. *Genetics* **93**: 13-35.

Heller RC, Kang S, Lam WM, Chen S, Chan CS, Bell SP. 2011. Eukaryotic origin-dependent DNA replication in vitro reveals sequential action of DDK and S-CDK kinases. *Cell* **146**: 80-91.

Houtkooper RH, Pirinen E, Auwerx J. 2012. Sirtuins as regulators of metabolism and healthspan. *Nat Rev Mol Cell Biol* **13**: 225-238.

Hu Y, Stillman B. 2023. Origins of DNA replication in eukaryotes. *Mol Cell* **83**: 352-372.

Ivy JM, Klar AJ, Hicks JB. 1986. Cloning and characterization of four SIR genes of Saccharomyces cerevisiae. *Mol Cell Biol* **6**: 688-702.

Kitada T, Kuryan BG, Tran NN, Song C, Xue Y, Carey M, Grunstein M. 2012. Mechanism for epigenetic variegation of gene expression at yeast telomeric heterochromatin. *Genes Dev* **26**: 2443-2455.

Klar AJ, Fogel S, Macleod K. 1979. MAR1-a Regulator of the HMa and HMalpha Loci in SACCHAROMYCES CEREVISIAE. *Genetics* **93**: 37-50.

Kobayashi T, Ganley AR. 2005. Recombination regulation by transcription-induced cohesin dissociation in rDNA repeats. *Science* **309**: 1581-1584.

Kwan EX, Alvino GM, Lynch KL, Levan PF, Amemiya HM, Wang XS, Johnson SA, Sanchez JC, Miller MA, Croy M et al. 2023. Ribosomal DNA replication time coordinates completion of genome replication and anaphase in yeast. *Cell Rep* **42**: 112161.

Kwan EX, Foss EJ, Tsuchiyama S, Alvino GM, Kruglyak L, Kaeberlein M, Raghuraman MK, Brewer BJ, Kennedy BK, Bedalov A. 2013. A natural polymorphism in rDNA replication origins links origin activation with calorie restriction and lifespan. *PLoS Genet* **9**: e1003329.

Larasati, Duncker BP. 2016. Mechanisms Governing DDK Regulation of the Initiation of DNA Replication. *Genes (Basel)* **8**.

Laughery MF, Hunter T, Brown A, Hoopes J, Ostbye T, Shumaker T, Wyrick JJ. 2015. New vectors for simple and streamlined CRISPR-Cas9 genome editing in Saccharomyces cerevisiae. *Yeast* **32**: 711-720.

Lewis JS, Gross MH, Sousa J, Henrikus SS, Greiwe JF, Nans A, Diffley JFX, Costa A. 2022. Mechanism of replication origin melting nucleated by CMG helicase assembly. *Nature* **606**: 1007-1014.

Li C, Mueller JE, Bryk M. 2006. Sir2 represses endogenous polymerase II transcription units in the ribosomal DNA nontranscribed spacer. *Mol Biol Cell* **17**: 3848-3859.

Li N, Gao N, Zhai Y. 2023. DDK promotes DNA replication initiation: Mechanistic and structural insights. *Curr Opin Struct Biol* **78**: 102504.

Linskens MH, Huberman JA. 1988. Organization of replication of ribosomal DNA in Saccharomyces cerevisiae. *Mol Cell Biol* **8**: 4927-4935.

Loo S, Rine J. 1994. Silencers and domains of generalized repression. *Science* **264**: 1768-1771.

Lynch PJ, Rusche LN. 2009. A silencer promotes the assembly of silenced chromatin independently of recruitment. *Mol Cell Biol* **29**: 43-56.

Mantiero D, Mackenzie A, Donaldson A, Zegerman P. 2011. Limiting replication initiation factors execute the temporal programme of origin firing in budding yeast. *EMBO J* **30**: 4805-4814.

Muller CA, Hawkins M, Retkute R, Malla S, Wilson R, Blythe MJ, Nakato R, Komata M, Shirahige K, de Moura AP et al. 2014. The dynamics of genome replication using deep sequencing. *Nucleic Acids Res* **42**: e3.

Neves-Costa A, Will WR, Vetter AT, Miller JR, Varga-Weisz P. 2009. The SNF2-family member Fun30 promotes gene silencing in heterochromatic loci. *PLoS One* **4**: e8111.

Pasero P, Bensimon A, Schwob E. 2002. Single-molecule analysis reveals clustering and epigenetic regulation of replication origins at the yeast rDNA locus. *Genes Dev* **16**: 2479-2484.

Ravindra A, Weiss K, Simpson RT. 1999. High-resolution structural analysis of chromatin at specific loci: Saccharomyces cerevisiae silent mating-type locus HMRa. *Mol Cell Biol* **19**: 7944-7950.

Remus D, Diffley JF. 2009. Eukaryotic DNA replication control: lock and load, then fire. *Curr Opin Cell Biol* **21**: 771-777.

Rhind N, Gilbert DM. 2013. DNA replication timing. *Cold Spring Harb Perspect Biol* **5**: a010132.

Rine J, Herskowitz I. 1987. Four genes responsible for a position effect on expression from HML and HMR in Saccharomyces cerevisiae. *Genetics* **116**: 9-22.

Rine J, Strathern JN, Hicks JB, Herskowitz I. 1979. A suppressor of mating-type locus mutations in Saccharomyces cerevisiae: evidence for and identification of cryptic mating-type loci. *Genetics* **93**: 877-901.

Rodriguez J, Lee L, Lynch B, Tsukiyama T. 2017. Nucleosome occupancy as a novel chromatin parameter for replication origin functions. *Genome Res* **27**: 269-277.

Salim D, Bradford WD, Freeland A, Cady G, Wang J, Pruitt SC, Gerton JL. 2017. DNA replication stress restricts ribosomal DNA copy number. *PLoS Genet* **13**: e1007006.

Schmid M, Durussel T, Laemmli UK. 2004. ChIC and ChEC; genomic mapping of chromatin proteins. *Mol Cell* **16**: 147-157.

Shahgaldi S, Kahmini FR. 2021. A comprehensive review of Sirtuins: With a major focus on redox homeostasis and metabolism. *Life Sci* **282**: 119803.

Singh J, Klar AJ. 1992. Active genes in budding yeast display enhanced in vivo accessibility to foreign DNA methylases: a novel in vivo probe for chromatin structure of yeast. *Genes Dev* **6**: 186-196.

Straight AF, Shou W, Dowd GJ, Turck CW, Deshaies RJ, Johnson AD, Moazed D. 1999. Net1, a Sir2-associated nucleolar protein required for rDNA silencing and nucleolar integrity. *Cell* **97**: 245-256.

Tanaka S, Nakato R, Katou Y, Shirahige K, Araki H. 2011. Origin association of Sld3, Sld7, and Cdc45 proteins is a key step for determination of origin-firing timing. *Curr Biol* **21**: 2055-2063.

Vasiljeva L, Kim M, Terzi N, Soares LM, Buratowski S. 2008. Transcription termination and RNA degradation contribute to silencing of RNA polymerase II transcription within heterochromatin. *Mol Cell* **29**: 313-323.

Viggiani CJ, Aparicio OM. 2006. New vectors for simplified construction of BrdU-Incorporating strains of Saccharomyces cerevisiae. *Yeast* **23**: 1045-1051.

Warner JR. 1999. The economics of ribosome biosynthesis in yeast. *Trends Biochem Sci* **24**: 437-440.

Weiss K, Simpson RT. 1998. High-resolution structural analysis of chromatin at specific loci: Saccharomyces cerevisiae silent mating type locus HMLalpha. *Mol Cell Biol* **18**: 5392-5403.

Woolford JL, Jr., Baserga SJ. 2013. Ribosome biogenesis in the yeast Saccharomyces cerevisiae. *Genetics* **195**: 643-681.

Yoshida K, Bacal J, Desmarais D, Padioleau I, Tsaponina O, Chabes A, Pantesco V, Dubois E, Parrinello H, Skrzypczak M et al. 2014. The histone deacetylases sir2 and rpd3 act on ribosomal DNA to control the replication program in budding yeast. *Mol Cell* **54**: 691-697.

Zentner GE, Kasinathan S, Xin B, Rohs R, Henikoff S. 2015. ChEC-seq kinetics discriminates transcription factor binding sites by DNA sequence and shape in vivo. *Nat Commun* **6**: 8733.

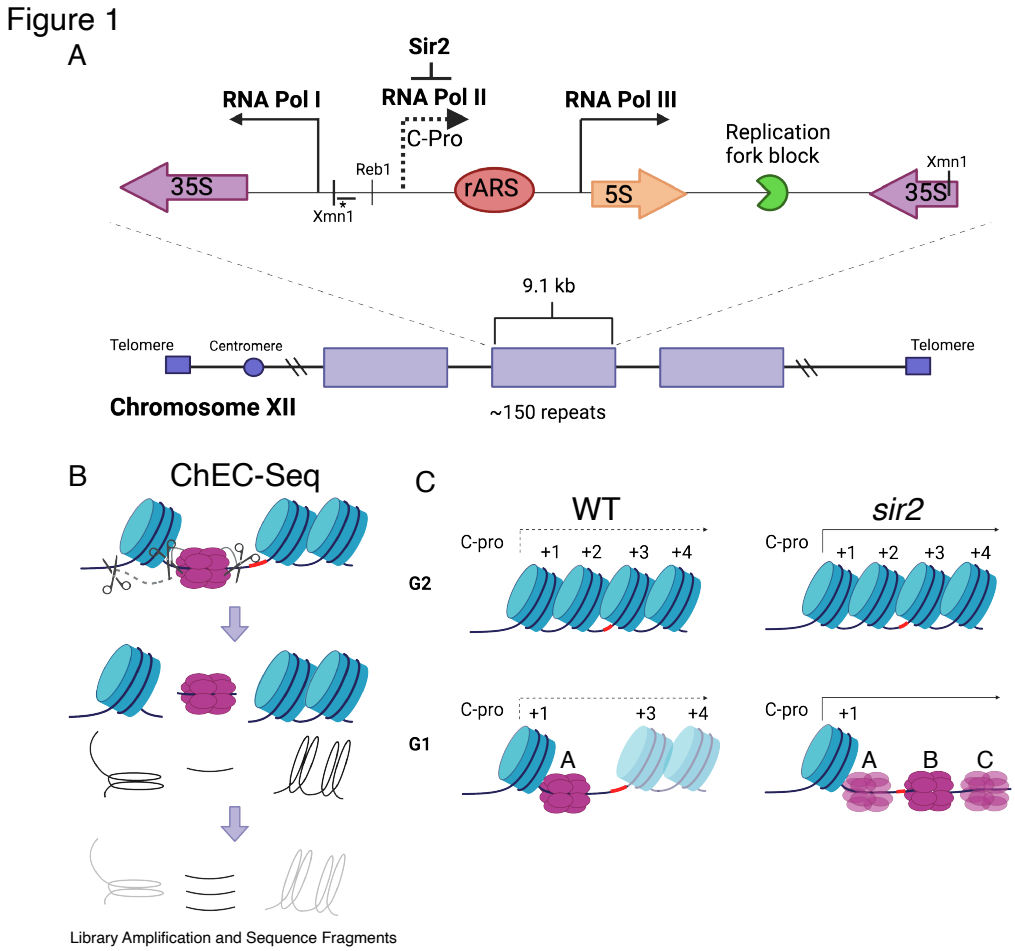

Figure 1. rDNA structure, Chromatin Endogenous Cleavage (ChEC), and MCM displacement in *sir2*. A. The 1.4 megabase rDNA region on chromosome XII is composed of approximately one hundred and fifty 9.1 kb repeats. Each repeat encodes both the 35S and 5S ribosomal RNAs (rRNA), which are transcribed by RNA Polymerase I (Pol I) and RNA Polymerase III (Pol III), respectively. The ribosomal origin of replication (rARS) is located between the 5' ends of these genes. The C-pro transcript, which is suppressed by Sir2, initiates approximately two hundred base pairs from the rARS. The unidirectional replication fork block, which functions to prevent collision between replication and transcription machinery, is depicted in green. The probe used in Southern blots in Figure 3 to assess licensing is marked by *. **B.** In ChEC-seq, micrococcal nuclease (MNase; depicted as scissors) is fused to the protein of interest, in this case MCM2. The double-hexameric MCM helicase complex, MCM2-7, is depicted in purple, and nucleosomes are in blue. Cleavage is induced by addition of calcium to permeabilized cells. Due to the proximity of nucleosome entrance and exit sites, MCM2-ChEC can reveal not only the binding site of the MCM complex but also that of the adjacent nucleosome. **C.** Depiction of nucleosomes and MCM complex in wild type and *sir2* in G1 and G2. Nucleosomes are numbered with respect to C-pro transcription. De-repression of C-pro transcription in *sir2* causes RNA PolII to displace the MCM complex to the right. The three different MCM helicase complexes depicted in the bottom right panel are intended to convey the three most prominent locations for the complex in *sir2*; this is not intended to indicate that there is ever more than one MCM complex in the same rDNA repeat. Created with BioRender.com.

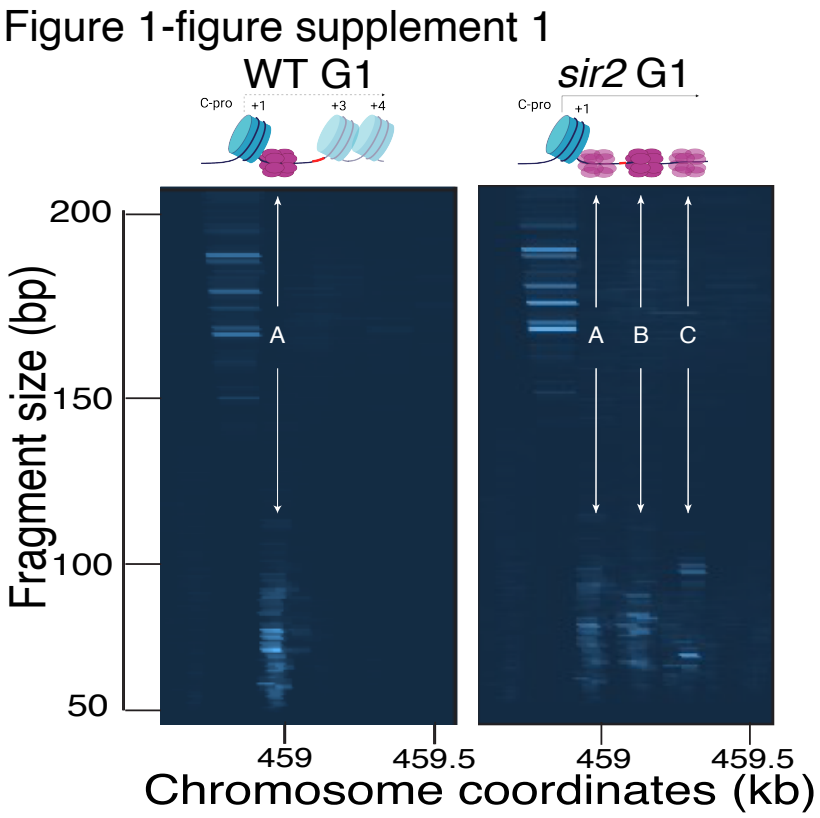

Figure 1-figure supplement 1. Computer-generated visualization of non-displaced and displaced MCM complexes, as determined by MCM2-ChEC. Sequencing reads from G1 cultures processed for MCM2-ChEC for wild type (16747) (left) and *sir2* (16769) (right) were plotted according to genomic location (x axis) and library insert size (y axis), with read depths indicated by color intensity. Note that these images are not agarose gels. The signal generated from inserts in the 50-100 base pair range (y axis) reflects the MCM complexes, whereas the signal from inserts in the 150-200 base pair range reflects the +1 nucleosome (see main text). De-repression of C-pro transcription in *sir2* causes RNA polII to push the MCM helicase complex from its normal location (arrow labeled "1") to the right, with the most prominent signals arising at the sites indicated by arrows labeled "2" and "3". Note that the presence of multiple MCM footprints in these composite images does not indicate that the presence of multiple MCM complexes in any individual repeat.

Figure 2

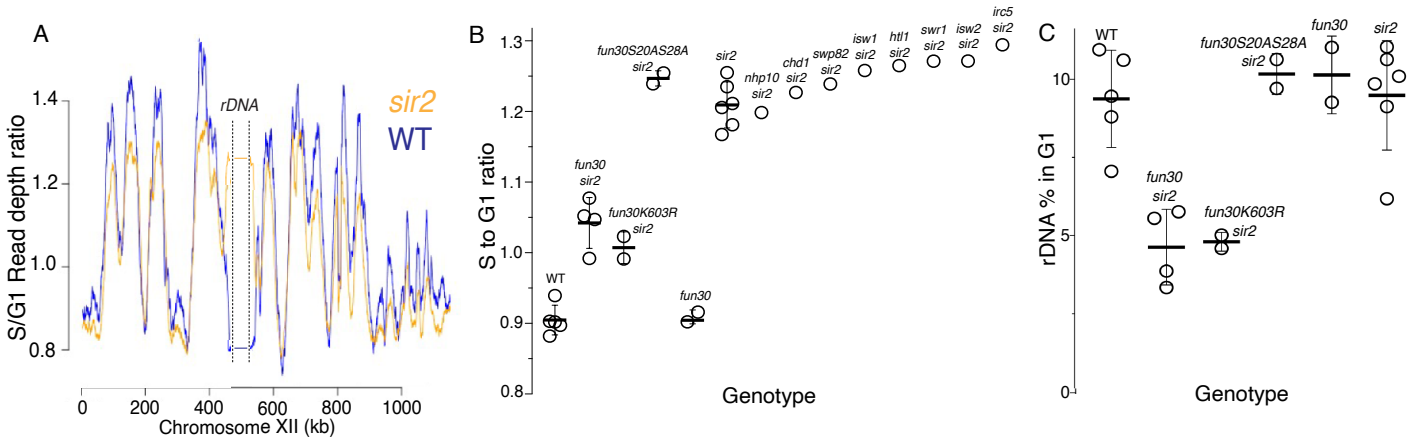

Figure 2. S-Seq applied to rDNA replication timing and copy number determination. A. S-seq replication profile of Chromosome XII. The region in the middle noted as the rDNA has been collapsed. Note that the rDNA replicates much earlier in *sir2* (16559) (orange) than in wild type (16535) (blue). **B.** rDNA replication timing in double mutants between *sir2* and various chromatin remodeling enzymes: *nhp10* (16729), *chd1* (16725), *swp82* (17061), *isw1* (16724), *htl1* (17059), *swr1* (16728), *isw2* (16673) and *irc5* (16723). *fun30-S20A S28A* (17113 and 17114) is non-phosphorylatable, and *fun30-K603R* (17345 and 17346) is catalytically inactive. The S to G1 ratio values (mean±SD) were 0.90±.0.02 for WT, 1.04±0.04 for *fun30sir2* (16909), 1.01±0.02 for *fun30K603R* and 1.21±0.03 for *sir2* ($p<0.001$ for WT vs *sir2*, *sir2* vs *fun30 sir2* and *sir2* vs *fun30K603Rsir2* using t-test). **C.** Effect of *sir2* and *fun30* mutation on rDNA size, as determined from the fraction of G1 sequencing reads that arise from 450-470 kb on chrXII. The values (% mean±SD) were 9.4±1.6 for WT, 4.6±1.2 for *fun30sir2*, 4.8±0.3 for *fun30K603R* and 9.2±1.8 for *sir2* ($p<0.001$ for WT vs *sir2* , *sir2* vs *fun30sir2* and *sir2* vs *fun30K603R sir2* using t-test)

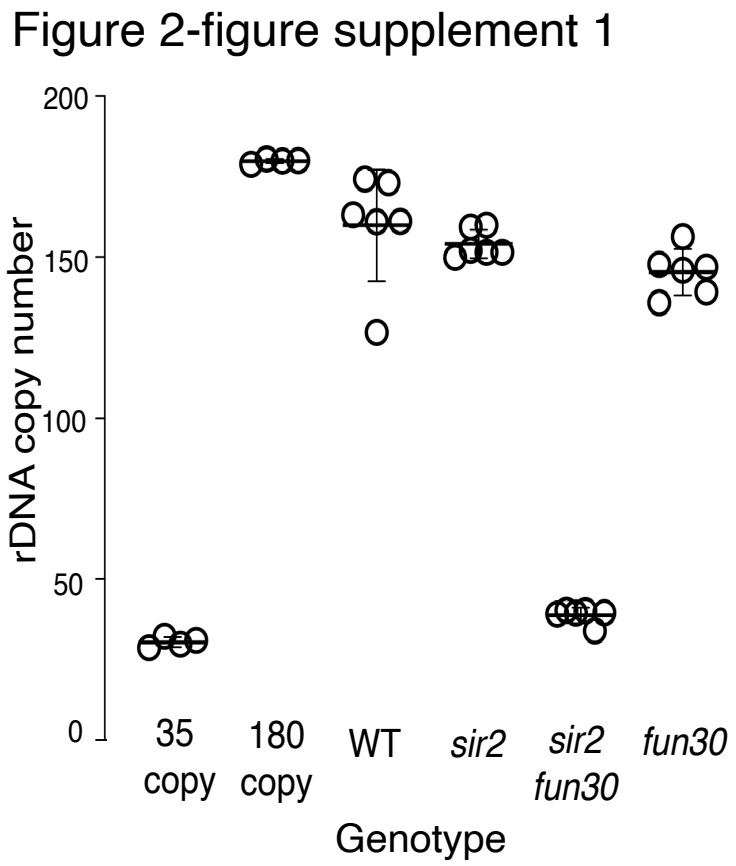

Figure 2-figure supplement 1. rDNA size as determined by qPCR. rDNA size for multiple isolates from each genotype were determined by qPCR, as described (Materials and Methods). Control strains with 35 (EK342) and 180 (EK68) copies of the rDNA were generated in *fob1* backgrounds to ensure copy number stability and were used as standards. Copy numbers were 160±7, 156±7, 38±3 and 147±7 for WT (14141), *sir2* (16668), *sir2 fun30* (17263) and *fun30* (17248), respectively ($p<0.001$ by t-test for *sir2* vs *sir2fun30*).

Figure 2-figure supplement 2

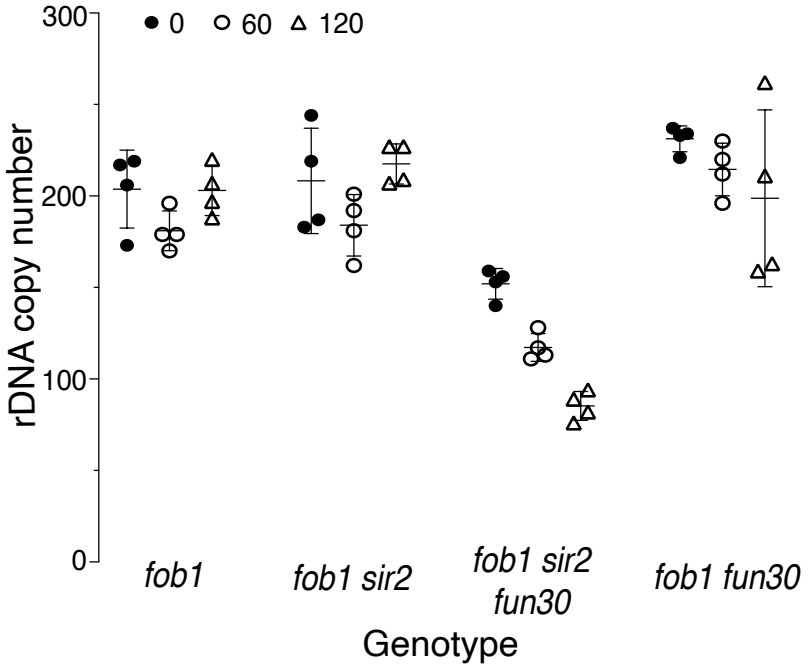

Figure 2-figure supplement 2. Changes in rDNA size of *fob1* strains with continuous passaging. Changes in rDNA size with passaging for 0 (closed circles), 60 (open circles) and 120 (open triangles) generations were determined by qPCR, as described (Materials and Methods) for the following genotypes (strain numbers in parentheses): *fob1 fun30* (17476), *fob1 sir2 fun30* (17548), *fob1* (17549), and *fob1 sir2* (17562). Control strains with 35 (EK342) and 180 (EK68) copies of the rDNA repeat were used as standards. The copy numbers (mean±SD) at 0, 60 and 120 divisions for different genotypes were as follows: 204±21, 191±22 and 203±14 for *fob1* (p NS by two-tailed t-test for any pairwise comparison); 208±29, 190±27 and 218±11 for *sir2 fob1* (p NS by t-test for any pairwise comparison); 152±8, 107±22 and 85±8 for *sir2 fun30 fob1* ($p < 0.001$ by t-test for any pairwise comparison); and 231±7, 225±28 and 199±48 for *fun30 fob1* (p NS by t-test for any pairwise comparison).

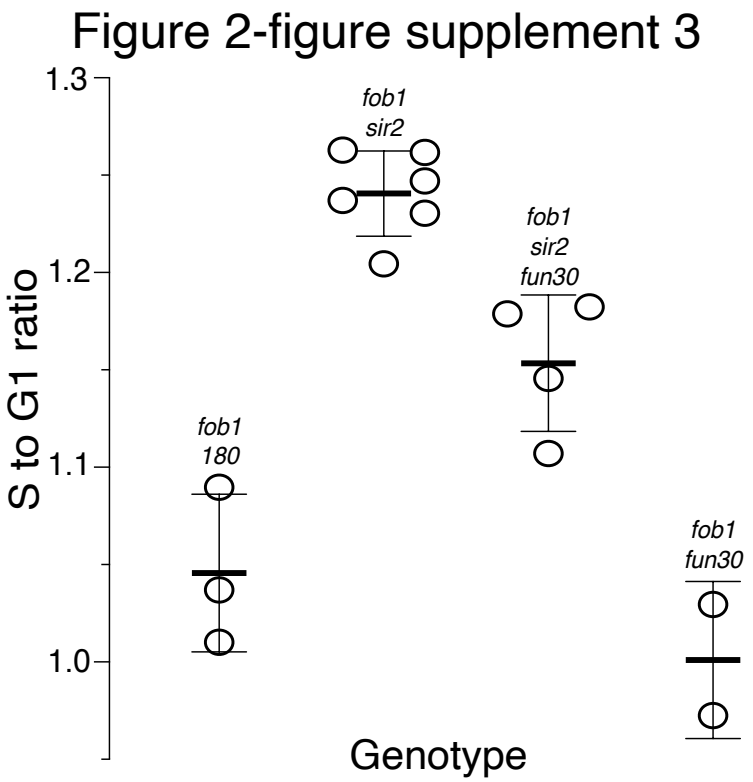

Figure 2-figure supplement 3. rDNA replication timing in *fob1* strains. Relative timing (Trel) of replication of the rDNA was determined as described in the main text. A value of 1 indicates that replication occurred at the genome-wide average; higher or lower values reflect earlier or later replication, respectively. Strains numbers used were as follows: *fob1* (16630, 17549, and 17550), *fob1 sir2* (17561), *fob1 sir2 fun30* (17548), and *fob1 fun30* (17477 and 17542). Trel values (mean±SD) were 1.05±0.04 for *fob1*, 1.24±0.02 for *fob1 sir2*, 1.15±0.04 for *fob1 sir2 fun30* and 1.00±0.04 for *fob1 fun30;* $p<0.01$ by t-test for *fob1 sir2* vs *fob1 sir2 fun30* and for *fob1* vs *fob1 sir2.*

Figure 3

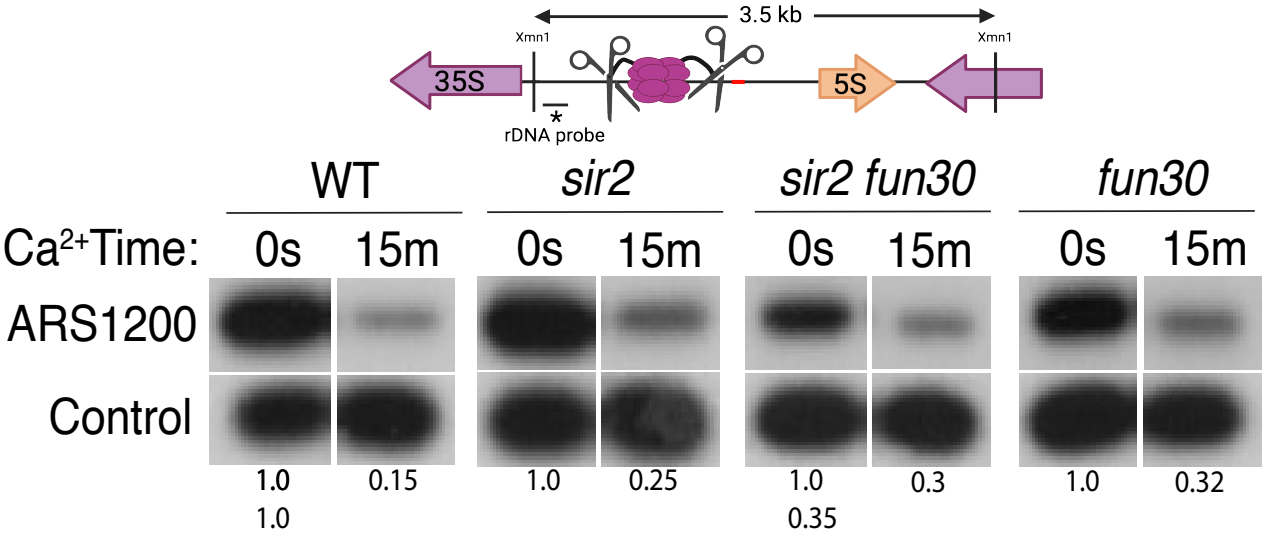

Figure 3. Licensing at the rARS, as determined by Southern blot. Activation of MCM-MNase in G1-arrested WT (16747), *sir2* (16769), *sir2fun30* (17257) and *fun30* (17256) cells at the rARS with calcium will eliminate the 3.5 kb XmnI fragment (upper panel). *PIK1*, a single-copy gene in which we detect no MCM binding, is used as a loading control. Normalized ARS1200 band intensity at 15m is expressed relative to time 0. Quantitation of the uncut band was used to infer relative rDNA array size in *sir2 fun30* mutant at 0.35 relative to WT.

Figure 3-figure supplement 1

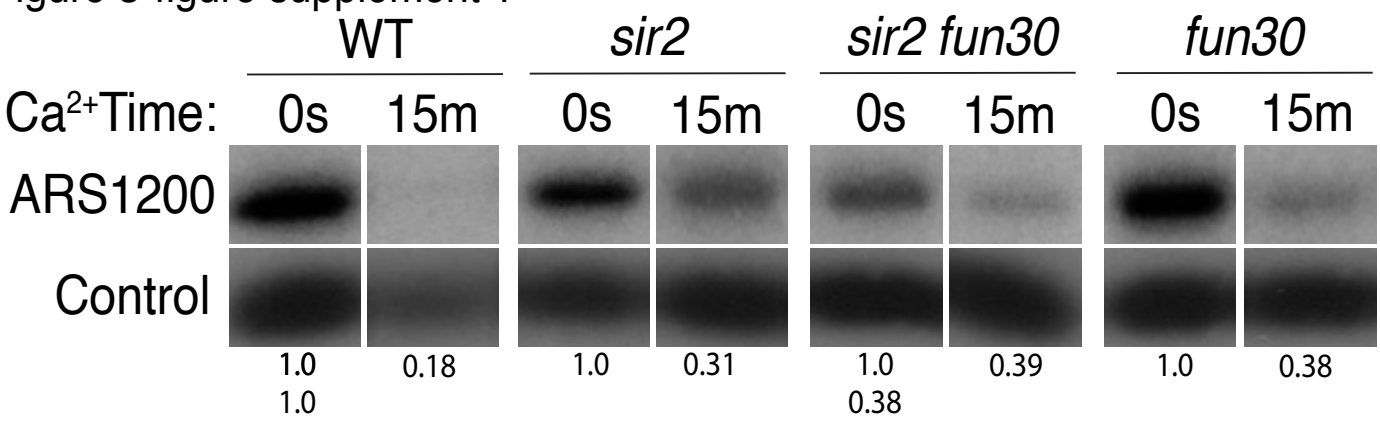

Figure 3- figure supplement 1. Licensing at the rARS using Southern blot (Replica of Figure 3). Activation of MCM-MNase in G1-arrested cells. PIK1 serves as a loading control. Normalized ARS1200 band intensity at 15 minutes is expressed relative to time 0. Quantitation of the uncut band was used to infer relative rDNA array size in *sir2 fun30* mutant at 0.38 relative to WT.

Figure 4

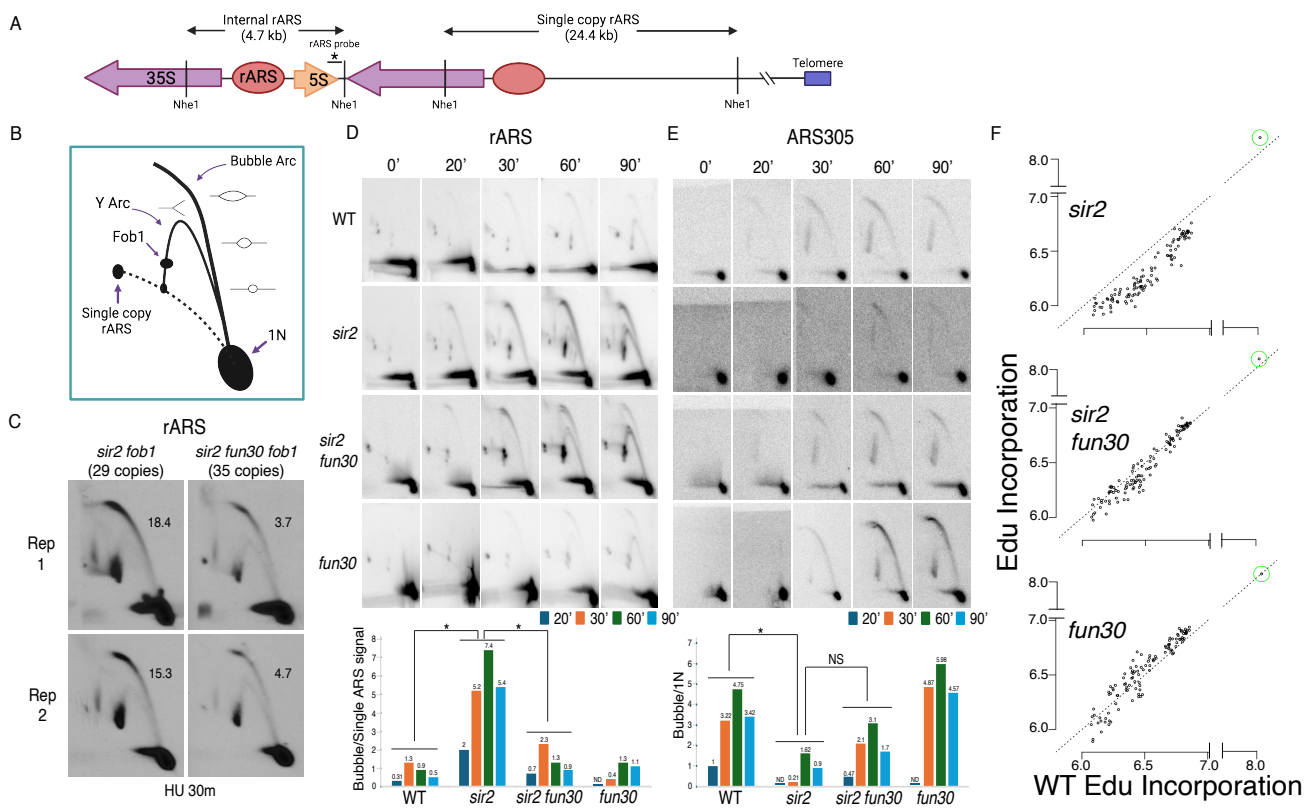

Figure 4. Deletion of *FUN30* suppresses origin activity at rDNA and promotes it elsewhere in the genome. **A.** Schematic of the right end of the rDNA locus depicting Nhe1 cut sites. Digestion with Nhe1 releases multiple copies of a 4.7 kb rARS-containing internal fragment (1N) and a single copy of a 24.4 kb fragment that contains the right-most rDNA origin. **B.** Diagram of replication structures detected by 2D gel. **C.** Replicas of 2D gels showing replication at the rDNA locus 30 minutes after release from alpha factor into HU in *sir2 fob1* (17564) or *sir2 fun30 fob1* (17556) strains with short (29 copies and 35 copies, respectively) rDNA arrays. Numbers indicate the ratio of bubble arc to single copy ARS signal, reflecting the number of activate origins per cell. The average number of activate origins (mean±SD) for *sir2 fob1* is 16.9±2.2 vs 4.2±0.7 ($P<0.05$ by t-test). **D.** 2D gels showing replication at the rDNA. Cells were arrested in G1 with alpha factor and then released into medium containing 200 mM HU. Quantitation of the ratio of bubble arc to 24.4 kb single copy rARS is shown below. * indicates significant differences ($p \leq 0.05$ as determined by comparing combined signals from all 4 time points by Student's t-test). Strain numbers used were as follows: wild type (16747), *sir2* (16769), *sir2 fun30* (17257) and *fun30* (17256). **E.** Replication of ARS305 was examined as in D, but the 1N spot was used for normalization and ratios of bubble arc to 1N spot were normalized to this ratio for the 20 minute time point in wild type. **F.** EdU incorporation at 111 early origins 1 hour after release from G1 into medium containing 200 mM HU. Total genome-wide read counts in each sample were normalized to the number of reads in the sample with the highest total, thereby normalizing numbers to genome-wide incorporation of EdU. Each dot represents a single origin, with read depths summed across a 5 kb window centered on the MCM binding site within each origin. Points are plotted according to EdU signal in wild type on the x axis and in the mutant in question on the y axis. Suppression of origin activity is reflected in points dropping below the dotted line at 45°. The rARS is circled in green. Strain numbers used were as follows: wild type (17265), *sir2* (17271), *sir2 fun30* (17279) and *fun30* (17281).

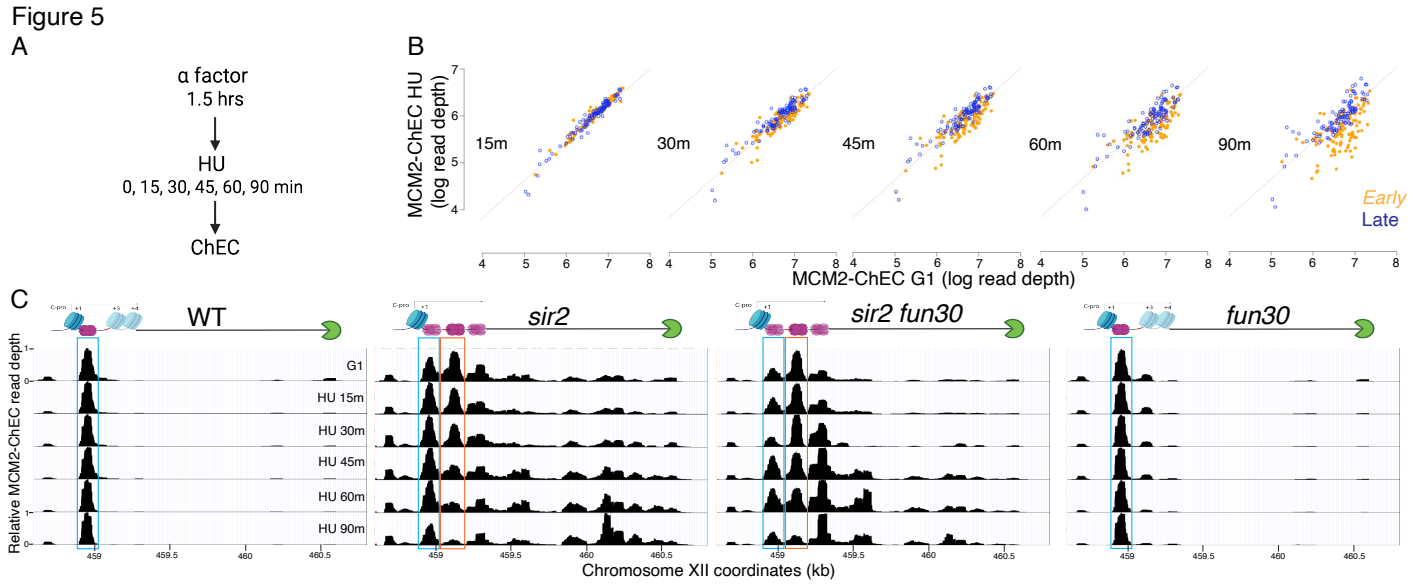

Figure 5. Disappearance of MCM2-ChEC signal can be used to monitor origin firing. A. Cells were synchronized in G1 phase using alpha factor for 1.5 hours before being released into media supplemented with hydroxyurea (HU). Cells were harvested at various time points post-release (15-90 minutes) and subjected to MCM2-ChEC analysis. **B.** Decrease in MCM2-ChEC signal in wild type (16747) for 111 early (orange) and 101 late (blue) origins. MCM2-ChEC signal was quantified over 200 base pair windows centered on the MCM binding site within each origin. Each point is plotted according to MCM2-ChEC signal at the time point in question on the y axis and the corresponding signal in G1 on the x axis, thus decrease in signal appears as a drop below the 45° diagonal. **C.** MCM signal at the rDNA. MCM2-ChEC signal in G1 appears predominantly at the location indicated by the blue rectangle seen in wild type (16747) and *fun30* (17256), whereas it is spread across both the blue and orange rectangles in the absence of Sir2. The displaced MCM2-ChEC signal (orange rectangle) in *sir2* (16769) disappears more rapidly than its non-displaced counterpart, and this effect is suppressed by *fun30* (17257). Decrease of MCM2-ChEC signal at the rARS is accompanied by increased signal to the right.

Figure 5- figure supplement 1

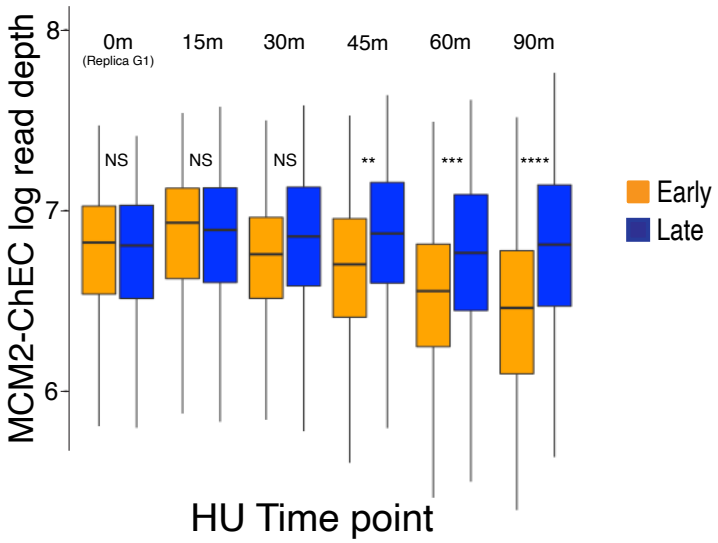

Figure 5-figure supplement 1. Quantification of MCM2-ChEC signal at 111 early (orange) and 101 late (blue) origins as cells progress through S phase (quantitation of Figure 5B). Cells were arrested in G1, released into medium containing 200 mM HU, and analyzed by MCM2-ChEC-seq at different time points. Total genome-wide read counts for each sample were normalized to the genome-wide read counts for the sample with the highest count. Strain is the same one used in Figure 5B. At each time point, we used Student's t test to determine MCM2-ChEC signal was different between early and late origins. Significance of two tail t-tests are abbreviated as "NS" (not significant), **($p \leq 0.01$), ***($p \leq 0.001$), and **** ($p \leq 0.0001$).

Figure 5- figure supplement 2

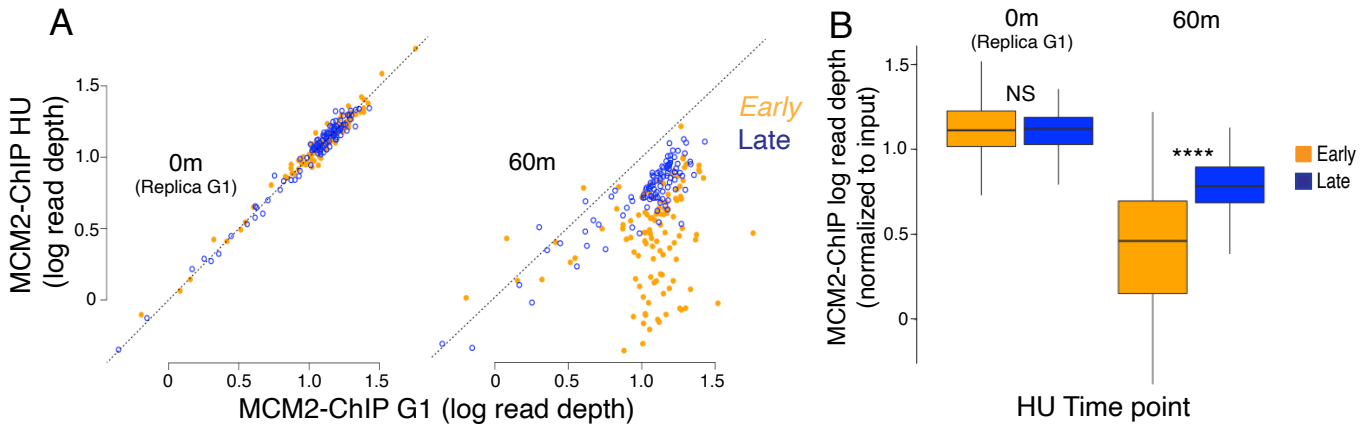

Figure 5-figure supplement 2. Quantitation of early and late origins using MCM2-ChIP. Chromatin-IP of FLAG-tagged MCM2 was used to measure levels of 111 early and 101 late origins in G1 and 60 minutes after release from G1 into medium containing 200 mM HU. Analysis was performed as done with MCM2-ChEC in Figure 5B and Figure 5-figure supplement 1. **A.** The MCM2-ChIP signal over a 200 base pair window at 111 early (orange) and 101 late (blue) origins in WT (17558) G1-arrested cells is compared to the signal in cells released into hydroxyurea for 60 minutes. The signal at early origins diminishes more than the signal at late origins. **B.** Box plots for MCM2-ChIP signal at early and late origins. P-values by two tail t-test for the signal abundance at early vs late origins: **** ($p \leq 0.0001$).

Figure 5- figure supplement 3

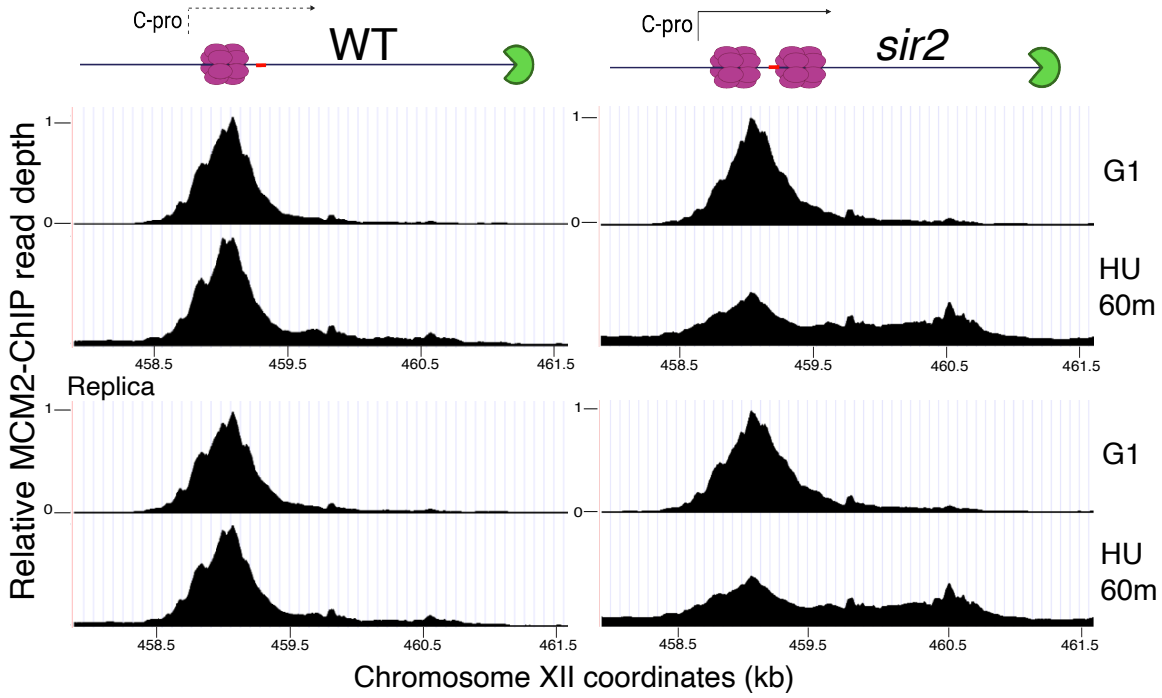

Figure 5- figure supplement 3. Change in localization of MCM2-ChIP signal at the rDNA with progression from G1 into S phase. Wild-type (left; strain 17558) and *sir2* (right; strain 17559) cells with FLAG-tagged MCM2 were arrested in G1 prior to release into media containing 200 mM HU and analyzed by ChIP. Relative MCM2-CHIP read depth is plotted according to chrXII coordinates. Diagrams at top show MCM double-hexamers in purple, the RFB in green, and the location of the C-pro transcript, either transcribed (solid line) or repressed (dotted line).

Figure 5-figure supplement 4

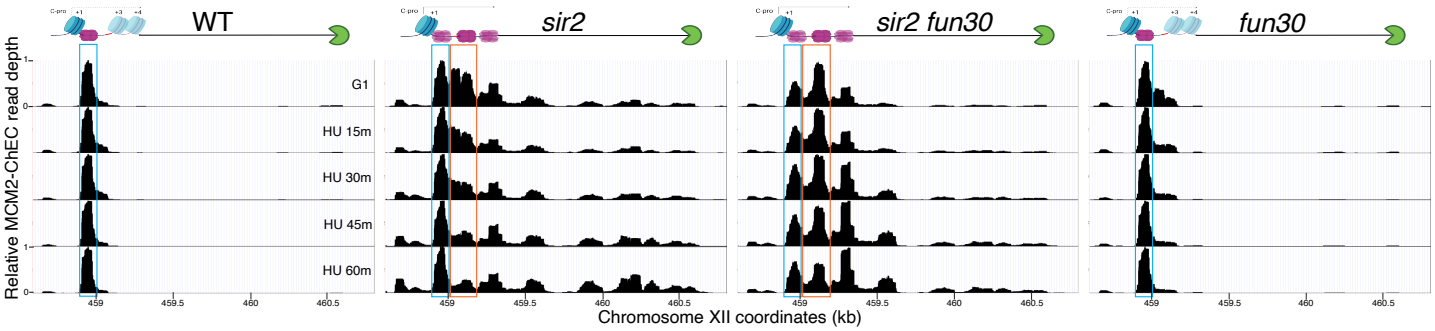

Figure 5-figure supplement 4. Deletion of *FUN30* suppresses activation of the displaced MCM complex at the rDNA (replica of results in Figure 5C). Each panel shows MCM2-ChEC data for cultures that were arrested in G1 and then released into medium containing 200 mM HU. Non-displaced and displaced MCM complexes are indicated by blue and orange rectangles, respectively. MCM2-ChEC data were quantified for the 51-100 base pair size range. Strains are the same as those used in Figure 5C. Diagrams at top show MCM double-hexamers in purple, the RFB in green, nucleosomes in blue, and the location of the C-pro transcript, either transcribed (solid line) or repressed (dotted line).

Figure 5-figure supplement 5

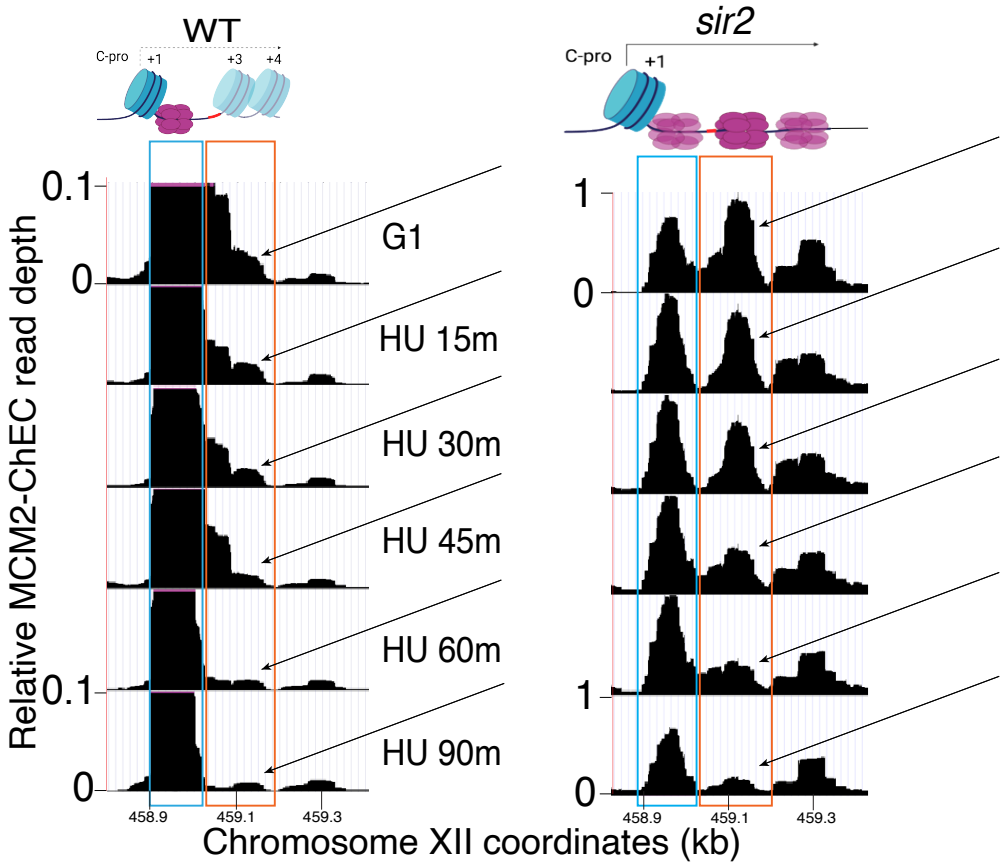

Figure 5-figure supplement 5. Displaced MCM complex is activated early in wild type. Enlarged region from figure 5C shows that, although only a small proportion of MCM complexes are displaced in WT (16747), this displaced population, indicated by arrows, is activated early, as is the case with in *sir2* (16769). Cartoons at top show nucleosomes in blue, MCM double-hexamers in purple, C-pro transcription, or lack thereof, as solid or dotted lines, respectively.

Figure 5-figure supplement 6

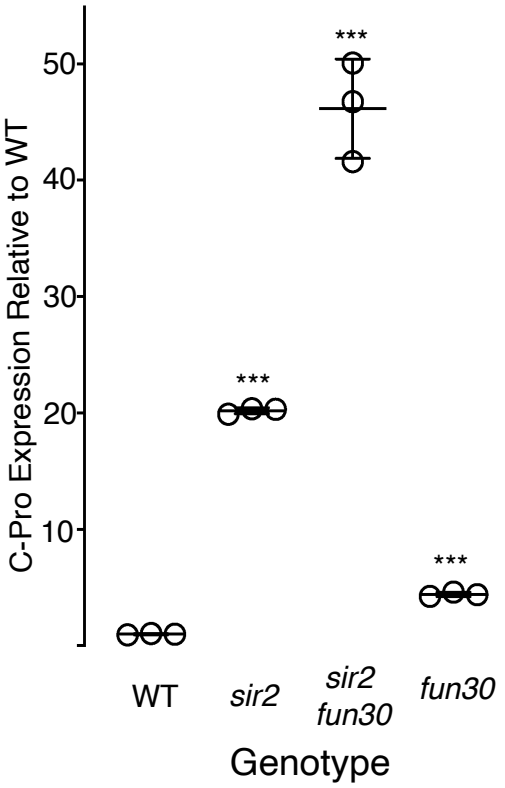

Figure 5-figure supplement 6. C-pro transcript levels. C-pro transcript levels in G1-arrested cells in *sir2* (16316), *sir2 fun30* (16727), and *fun30* (16711) were measured in triplicate using qPCR and expressed relative to WT (14141). All values are normalized to rDNA array size. *** denotes $p<0.001$ for comparison with WT using t-test.

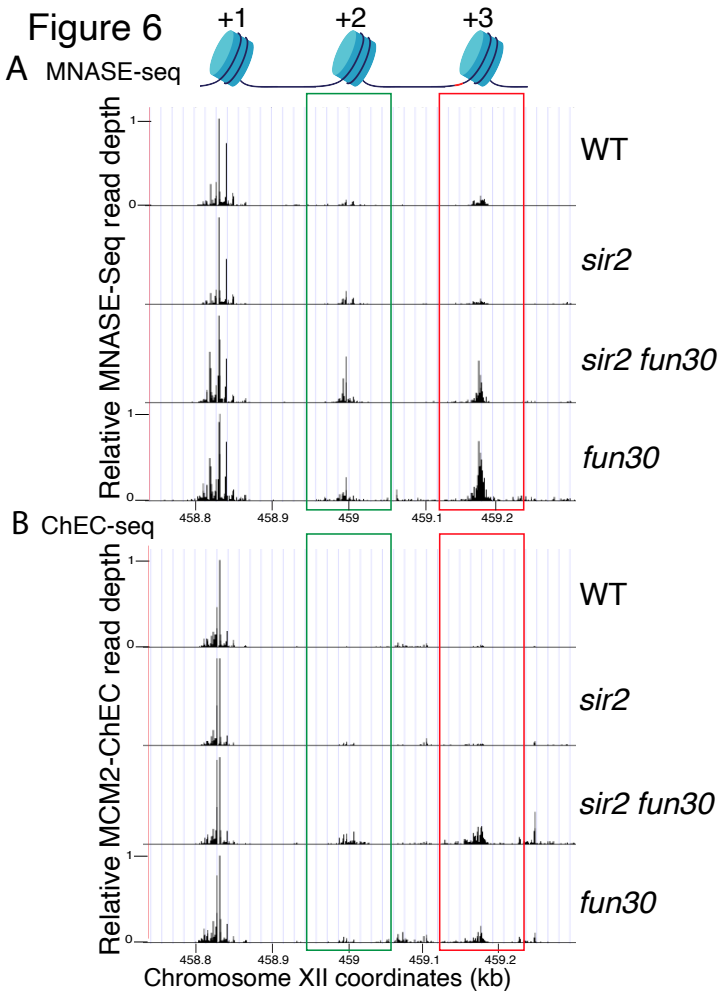

Figure 6. Nucleosome occupancy assessed by MNase-seq and MCM2-ChEC. A. Analysis of nucleosome occupancy at rDNA origins using MNase-seq revealed a consistent high occupancy of the +1 nucleosome across WT (16747), *sir2* (16769), *sir2 fun30* (17257) and *fun30* (17256), which served as our normalization reference. Occupancy at the +2 (green box) and +3 (red box) positions was increased by deletion of *FUN30* in both *sir2* and *SIR2*. MCM2-ChEC signal was quantified specifically from the 151-200 base pair (nucleosome) size range. **B.** Analysis of nucleosome occupancy with MCM2-ChEC (see Figure 1B) reveals nucleosome occupancy in that subset of cells and rDNA repeats in which MCM is present. Deletion of *FUN30* leads to increased occupancy at the +2 and +3 positions in a *sir2* background. MCM2-ChEC signal was quantified specifically from the 151-200 base pair (nucleosome) size range.

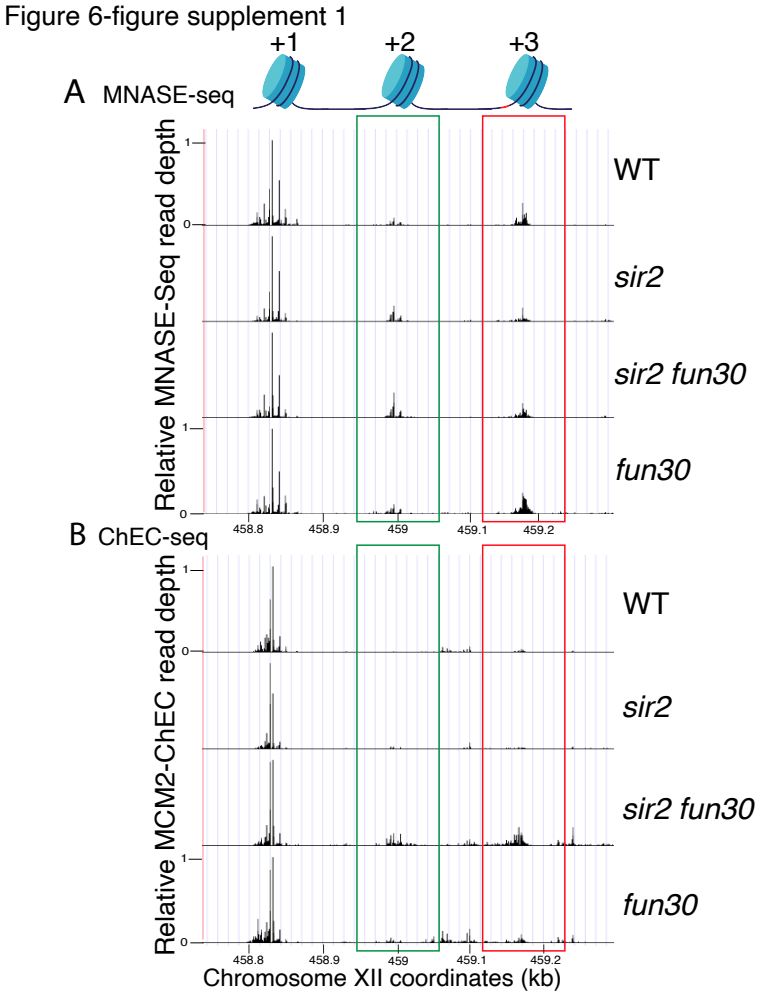

Figure 6-figure supplement 1. Nucleosome occupancy assessed by MNase-seq and MCM2-ChEC (Replica of Figure 6). A. MNase-seq analysis of nucleosome occupancy at rDNA origins Deletion of *FUN30* increased occupancy at +2 (green) and +3 (red) positions in both *sir2* and *SIR2* backgrounds. Strains are the same as those used in Figure 6. **B.** MCM2-ChEC analysis confirmed that *FUN30* deletion increases +2 and +3 nucleosome occupancy in a *sir2* background.

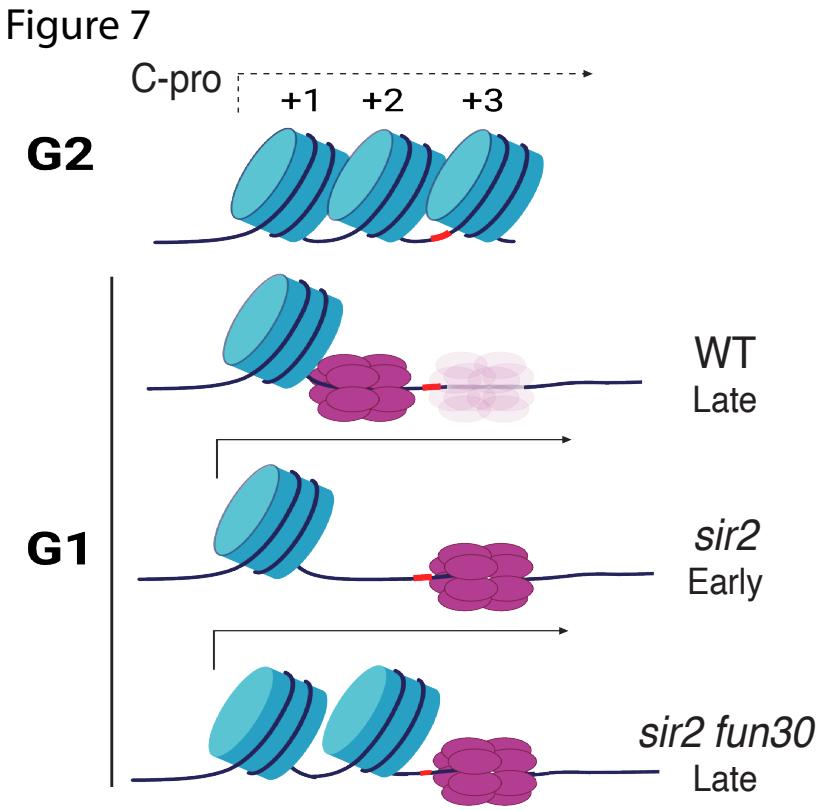

Figure 7. Model for relationship between MCM location and replication timing at the rDNA. MCM helicase complex (purple ovals) in wild type abuts the +1 nucleosome (blue cylinder) in G1, making it relatively resistant to activation. Deletion of *SIR2* derepresses C-pro transcription (arrow pointing to the right), and RNA PolII pushes MCM complex to a nucleosome free area, where it is more prone to activation. Deletion of *FUN30* in a *sir2* mutant leads to increased nucleosome occupancy at the +2 position, adjacent to MCM complex, making this complex resistant to activation. Short red stretch of DNA (e.g. between +2 and +3 nucleosomes in top row) indicates ACS. "Ghost" Mcm complex in wild type indicates the small fraction of Mcm that is displaced even in wild type cells (see Figure 5-figure supplement 5). Created with BioRender.com.